Design of an Offshore Wind Turbine Monopile Foundation

Meng Yuan Kuok

Exeter College

FINAL HONOUR SCHOOL OF ENG

DECLARATION OF AUTHORSHIP

You should complete this certificate. It should be bound into your fourth year project report, immediately after your title page. Three copies of the report should be submitted to the Chairman of examiners for your Honour School, c/o Clerk of the Schools, examination Schools, High Street, Oxford.

Name (in capitals): ……

College (in capitals): …… **Supervisor:** ……

Title of project (in capitals): ……..……

Page count (excluding risk and COSHH assessments): ……

Please tick to confirm the following:

I have read and understood the University's disciplinary regulations concerning conduct in examinations and, in particular, the regulations on plagiarism (*The University Student Handbook. The Proctors' and Assessors' Memorandum, Section 8.8*; available at https://www.ox.ac.uk/students/academic/student-handbook) ☐

I have read and understood the Education Committee's information and guidance on academic good practice and plagiarism at https://www.ox.ac.uk/students/academic/guidance/skills. ☐

The project report I am submitting is entirely my own work except where otherwise indicated. ☐

It has not been submitted, either partially or in full, for another Honour School or qualification of this University (except where the Special Regulations for the subject permit this), or for a qualification at any other institution. ☐

I have clearly indicated the presence of all material I have quoted from other sources, including any diagrams, charts, tables or graphs. ☐

I have clearly indicated the presence of all paraphrased material with appropriate references. ☐

I have acknowledged appropriately any assistance I have received in addition to that provided by my supervisor. ☐

I have not copied from the work of any other candidate. ☐

I have not used the services of any agency providing specimen, model or ghostwritten work in the preparation of this project report. (See also section 2.4 of Statute XI on University Discipline under which members of the University are prohibited from providing material of this nature for candidates in examinations at this University or elsewhere: http://www.admin.ox.ac.uk/statutes/352-051a.shtml.) ☐

The project report does not exceed 50 pages (including all diagrams, photographs, references and appendices). ☐

I agree to retain an electronic copy of this work until the publication of my final examination result, except where submission in hand-written format is permitted. ☐

I agree to make any such electronic copy available to the examiners should it be necessary to confirm my word count or to check for plagiarism. ☐

Candidate's signature: …….. **Date:** ……..

1. Abstract

For wind energy to compete with traditional sources of energy like fossil fuels, large cost reductions have to be made in the development of wind farms. The need for greater efficiency, the availability of land, and other considerations have resulted in offshore wind turbines increasing in scale and moving further offshore into deeper water. Monopiles are the most popular offshore wind turbine foundation and currently hold a lot of potential for cost reduction; traditional monopile design methods, such as the American Petroleum Institute (API) method, have been proven to be overly conservative and inaccurate for the new generation of large diameter monopiles. Thus, new design methods like the Pile Soil Anaysis project (PISA) method have arisen that aim to address these issues.

The aim of this project is to compare the current monopile design method of API to the new design method proposed within the PISA project, and to explore how the methods and their designs evolve with increasing scale and water depth. Using a limit state design methodology, the two design methods were used to design monopiles for three theoretical wind turbines of 10, 12 and 15MW in offshore clay design scenarios of water depths ranging from 30 to 50m. The scale of the theoretical wind turbines currently exceed any existing models and were used in order to investigate the differences and future potential of both design methods. MATLAB code was developed for the project to model the static and dynamic response of wind turbines, thus aiding the design process by assessing, for a given monopile foundation, whether a wind turbine satisfies the limit state requirements.

Contents

2. Introduction

The demand for offshore wind turbines is increasing due to the drive towards clean, renewable energy. However, due to the competitiveness of the cost of traditional sources of energy such as fossil fuels, significant cost reductions in the production of wind energy are required for it to become economically viable (Byrne et al., 2017).

2.1 The Problem

Wind turbines can be built onshore, but considerations such as landscape aesthetics, availability of land and noise pollution have led to them being built offshore in shallow sea level areas. Unfortunately, the cost of offshore wind turbines is approximately twice that of their onshore counterparts and the UK government aims to reduce the lifetime cost of an offshore wind farm per unit of energy by 28.6%, from 140/MWh to 100/MWh by the year 2020, to make offshore wind energy comparable to the traditional sources. Possible solutions to the problem are to increase the scale of the wind turbines and to site wind farms further offshore for better wind conditions; these solutions rely heavily on the development of cost-efficient foundations. 75% of existing foundations of offshore wind turbines are single monopiles with diameters of around 5-6m. Monopiles are a type of cylindrical, large diameter, open-ended pile, and are a popular offshore wind turbine foundation in relatively shallow water of up to around 35m depth. While wind turbines have been constructed in depths up to 70m using jacket, tripod and floating foundations, they are less economical due to the monopile's competitive fabrication and installation costs, and its robustness in most soil conditions (Kallehave et al., 2015). Currently, monopiles up to around 8m in diameter have been used for water depths of up to around 40m (Haiderali and Madabhushi, 2013), and future designs are planned for diameters of 10m and more (Hermans and Peeringa, 2016). In addition, manufacturing capabilities for monopiles of up to 11m in diameter and 120m in length are being developed which are expected to be able to carry 8MW wind turbines (Sif, n.d.). A breakdown and analysis of cost by Junginger and Faaij (2004) showed that around 70% of the price of offshore wind energy is due to initial investment costs, of which 20% is the monopile manufacture and 30% is due to transportation and installation of the wind turbine. A significant portion of the installation cost is due to the pile driving using hydraulic hammers. The most popular current design method for laterally loaded monopiles is the traditional semi-empirical *p-y* method, used in offshore design codes like American Petroleum Institute (API) and Det Norske Veritas (DNV), but it is now considered overly conservative and outdated, having been originally designed for slim jacket piles of large length to diameter ratios for the offshore oil and gas industry.

Newer, larger wind turbines are requiring monopiles of smaller length-to-diameter ratios and there are concerns, backed by research, that the *p-y* method is no longer appropriate (Byrne et al., 2015). Thus, with the rising scale and depth of offshore wind turbines, there stand to be large savings if the degree of conservatism can be reduced in monopile design and if individually optimised monopiles are produced for each position in a wind farm to accommodate for local variations of conditions. New design methods have been developed, such as those by PISA (Pile Soil Analysis), a joint industry project, to tackle the problem.

2.2 Project Overview

The aim of the project is to design monopiles using the traditional *p-y* method (which will be referred to as the API method) and the newer PISA design method for offshore design scenarios in order to compare the cost-efficiency of both methods, to establish whether the claims of conservatism of the p-y method are justified, and to examine the future potential of the two design processes. The design scenarios consist of a clay soil profile from Cowden in North England (which is referred to as the Cowden Till soil profile), determined by PISA to be representative of an offshore clay profile, with various depths and wind turbine power ratings. Three wind turbines of 10, 12 and 15MW were considered in water depths of 30-50m: the 10MW wind turbine was based on the Technical University of Denmark's 10MW Reference Wind Turbine (Bak et al., 2013), which is referred to as the DTU 10MW RWT, with modifications from the Energy Research Centre of The Netherlands (ECN), from which the 12MW and 15MW wind turbines were directly scaled.

MATLAB code was developed to model a given monopile's static and dynamic response to aid the design process. A Static Analysis Code (SAC) was written that uses a previously developed program called OxPile (Burd, McAdam and Abadie) which is capable of modelling the static response of a wind turbine using both API and PISA methods. A complementary Eigen Analysis Code (EAC) was written to model the dynamic response of the wind turbine. Finally, a Combined Analysis Code (CAC) was developed to tie the SAC and EAC together, selecting an optimised foundation design following API and PISA methods in a given geometric parameter space using a limit state design methodology. Using the data and results obtained by the Combined Analysis Code (CAC), the two design methods are compared and analysed, and an understanding of the design methods is developed.

3. Literature Review

The simplified form of an offshore monopile founded wind turbine is shown in Figure 1. The rotor blades of the wind turbine are connected to a shaft that runs through the hub, into the nacelle, which

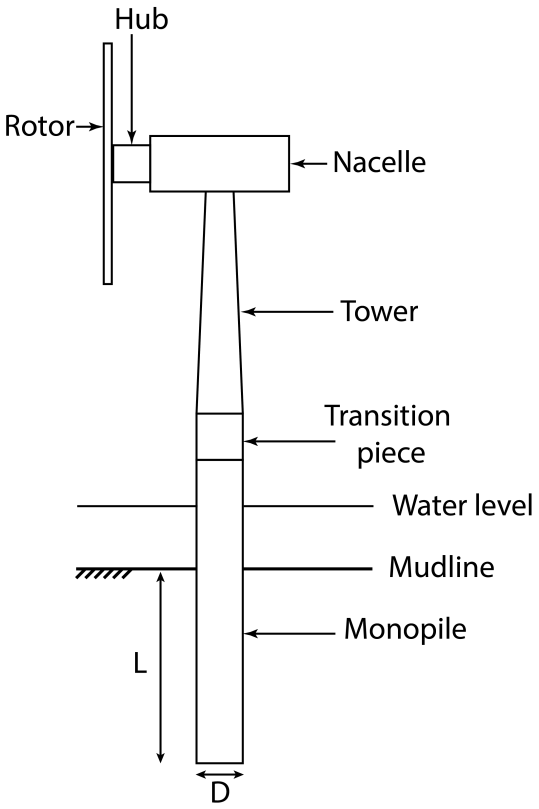

Figure 1: Diagram of an offshore, monopile founded wind turbine

Parameter	**Symbol**	**Non-dimensionalised Parameter**	**Non-dimensionalised Expression**
Diameter	D		
Embedded Length	L	Aspect Ratio	L/D
Wall Thickness	t	Thickness Ratio	D/t

Table 1: Monopile parameters and non-dimensionalised forms

houses the generator and gearbox. The tower is the above-water support structure for the energy generating components; the transition piece connects the tower to the monopile.

3.1 Monopiles

Monopiles are cylindrical, open-ended piles made from steel. As offshore foundations, they experience axial loading from self-weight of the structure as well as lateral loading and bending moments from wind and wave forces. The key monopile parameters and their non-dimensionalised forms are shown in Table 1; monopile parameters will be referred to predominantly in their non-dimensionalised forms. It should be noted that D is a measure of the outside diameter.

Ultimate Limit State (ULS)	Corresponds to the maximum load-carrying resistance
Fatigue Limit State (FLS)	Corresponds to failure due to the effect of dynamic loading
Accidental Limit State (ALS)	Corresponds to the maximum load-carrying capacity for accidental loads
Serviceability Limit State (SLS)	Corresponds to tolerance criteria applicable to normal use

Table 2: DNV limit states (DNV-GL, 2016)

3.2 Limit State Methodology

Current guidelines for wind turbine design like DNV and API use a limit state methodology in their design approach. The DNV defines a limit state as "a condition beyond which a structure or structural component will no longer satisfy the design requirements" (DNV-GL, 2016) and considers the limit states shown in Table 2; the limit states considered in this project are the ULS and FLS. The ULS is concerned with the ultimate loads on the structure and the limit state is generally exceeded through failure of either the structure or the soil. The FLS is concerned with the dynamic loads on

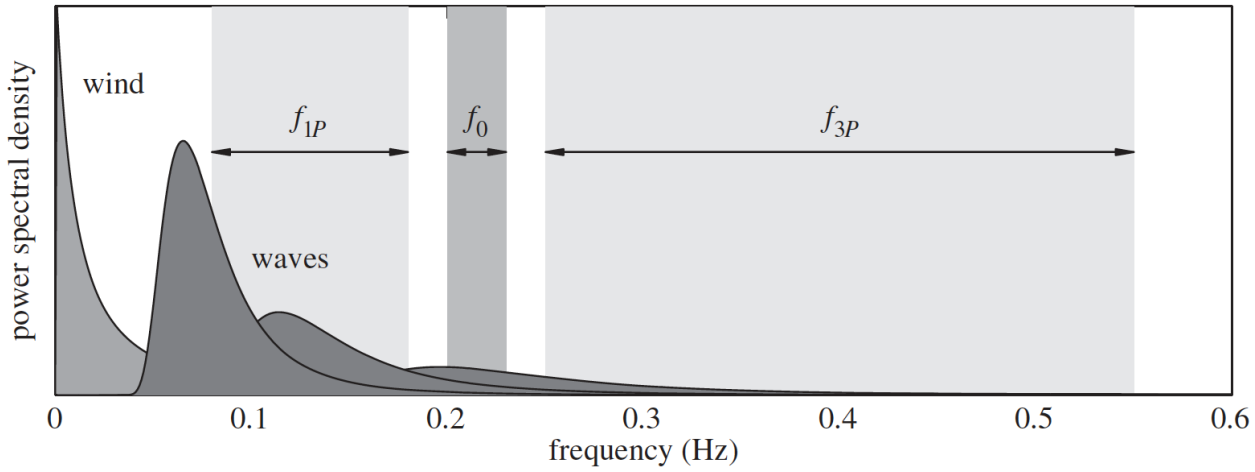

Figure 2: Typical excitation ranges for an offshore wind turbine (Kallehave et al., 2015)

the structure and the resulting cumulative damage over the wind turbine's service life. Offshore wind turbines experience environmental and operational cyclic loads; the environmental loads arise from wind and waves and the operational loads are a result of the rotation of the rotor blades. Thus, in order to prevent the development of fatigue damage, the wind turbine must be designed such that its natural frequency does not coincide with the frequency ranges of the dynamic loads; an example of the frequency ranges are shown in Figure 2. The 1P range is due to the rotational frequency of the rotor and ranges from the minimum to maximum rotor speed in Hertz. The 3P range is due to

ULS	Requirement 1 (yield)	The design yield strength is not exceeded at any point
ULS	Requirement 2 (displacement)	The lateral displacement (ν_g) at the seabed does not exceed a maximum deflection value.
FLS	Requirement 3 (natural frequency)	The fundamental natural frequency (ω_0) of the wind turbine falls within a defined range of the optimum natural frequency

Table 3: Summarised monopile limit state requirements for this project

the individual blade-passing frequency and is the 1P range multiplied by 3 (for the number of turbine blades). Wind turbines are typically designed to be soft-stiff structures so that they fall in the f_0 range and thus avoid the majority of the main loading frequencies (Kallehave et al., 2015). Offshore wind turbines are generally expected to have a service life of around 25 years and the prediction of fatigue damage is usually calculated using design load cases and stochastic methods.

Due to the scope of this project, only the ultimate limit state and fatigue limit state were considered in the design of the monopiles. The ULS was considered in terms of yielding of the structure and failure of the soil. The FLS was addressed by ensuring the wind turbine's fundamental frequency did not overlap with the frequencies of the dynamic loading, so that fatigue damage was minimised; using design load cases to calculate service life and fatigue damage was outside the project's scope. The limit states were thus summarised into the three requirements shown in Table 3.

3.3 API *p-y* Method

The *p-y* method is based on the Winkler (1867) approach which assumes the pile acts as a beam supported by a series of uncoupled springs; the model is shown in Figure 3 along with an example of the *p-y* curves. The original *p-y* curves were developed by Reese et al. (1974) and Matlock (1970), and were based on empirical results and theoretical predictions of steel tubes of diameter $D = 610$mm with an aspect ratio of $D/t = 34$. The non-linear *p-y* curves define the soil reaction p at a given depth as a function of the lateral displacement y. The continuous piecewise curves were assembled from four discrete parts: a straight line, a parabola, a linear portion and finally a constant value of ultimate strength (Doherty and Gavin, 2012). The *p-y* method was developed and used predominantly for oil and gas structures with piles of similar aspect ratios to the test piles, however, they have recently been extrapolated for large diameter monopiles of smaller aspect ratios. Current monopiles are much stouter, with aspect ratios of around 3-6 and so concerns have arisen about

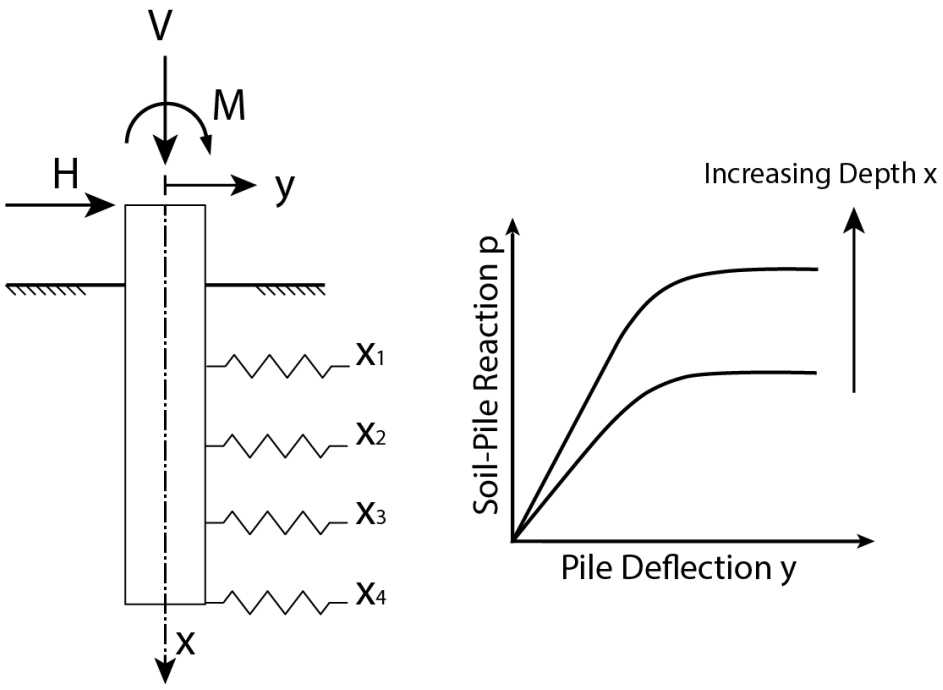

Figure 3: API method monopile soil reactions (left) and *p-y* curves (right) (Pando et al., 2006)

the method's suitability for extrapolation; new verification is required for the API *p-y* method. Studies of the *p-y* method show that it does indeed underestimate the soil reactions of monopiles in some soil types (Bisoi and Haldar, 2014) and hence significantly overestimates the lateral displacement and rotation at mudline (Haiderali and Madabhushi, 2013). This poses additional concerns about calculations of the ULS and the natural frequency of the wind turbine, which would mean incorrect calculations of service life and fatigue damage.

3.3.1 *p-y* Formulae

The formulae for *p-y* spring stiffness is obtained from the DNV-GL (2016) guidelines which recommends for piles in cohesive clay soils that the static ultimate lateral resistance be calculated from:

$$p_u = \begin{cases} (3s_u + \gamma' X)D + Js_u X & \text{for } 0 < X \leq X_R; \\ 9s_u D & \text{for } X > X_R. \end{cases} \tag{3.1}$$

Where X is the depth, D is the monopile diameter, and X_R is the transition depth below which the value of $(3s_u + \gamma' X)D + Js_u X$ exceeds $9s_u D$. Soil parameters γ', J and s_u are defined in Section 6.4. The *p-y* curve can then be generated using the expressions:

$$p = \begin{cases} \frac{p_u}{2}(\frac{y}{y_c})^{\frac{1}{3}} & \text{for } y \leq y_c; \\ p_u & \text{for } y > y_c. \end{cases} \tag{3.2}$$

Where $y_c = 2.5\epsilon_{50}D$; ϵ_{50} is another soil parameter described in Section 6.4. The DNV guidelines then state that the first discretisation point beyond the origin may be localised at the relative displacement

$\frac{y}{y_c} = 0.1$; this approximation removes the need to solve for lateral displacement to obtain the value of p and gives the initial soil stiffness for small lateral displacements.

3.4 PISA Method

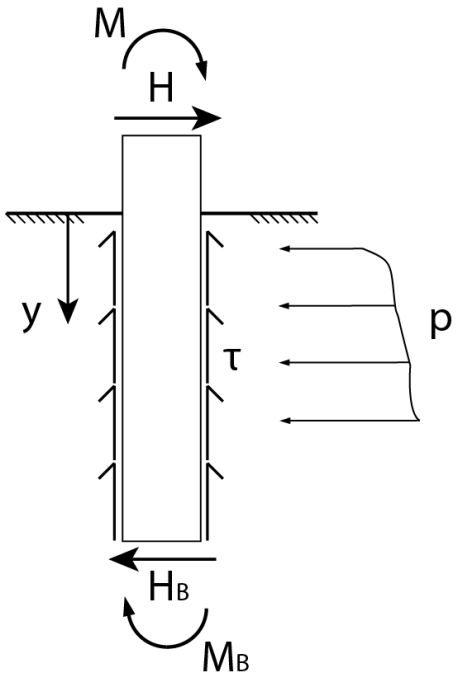

Figure 4: PISA method monopile soil reaction components

The joint industry project PISA developed their new design method specifically for offshore wind turbines through theoretical modelling and empirical testing, with the project focused on being able to apply the method to any soil or clay profile (Byrne et al., 2015). The key differences between the API and PISA methods are the calculations of soil stiffness and the soil reaction components used in their models; previous research (e.g. Davidson, 1982 and Lam and Martin, 1986) has shown that caissons, of similar geometries to offshore monopiles, are subject to additional soil reactions. Thus, the PISA design method is based on extensions of the *p-y* method and has proposed 3 additional components of soil reaction for short, large diameter monopiles. The four separate components of soil reaction are shown in Figure 4 and are given as:

- A distributed load p along the embedded pile shaft, similar to the *p-y* method but with a different formulation
- A distributed moment m applied to the embedded pile shaft as a result of vertical shear stresses τ developed on the shaft
- A shear force H_B applied on the base
- A moment M_B applied on the base

Parameter	Range
Diameter D (m)	5-10
Aspect Ratio L/D	2-6
Thickness Ratio D/t	60-110

Table 4: PISA project geometric parameter space (Byrne et al., 2015)

Soil Component	Formula
Lateral stiffness (per unit length of monopile)	$\frac{dp}{dv} = k_p G$
Rotational stiffness (per unit length of monopile)	$\frac{dm}{d\psi} = k_m G D^2$
Base shear stiffness	$\frac{dH_B}{dv} = k_H D G$
Base rotational stiffness	$\frac{dM_B}{d\psi} = k_M G D^3$

Table 5: PISA soil components stiffness formulae

As part of the development and verification of the PISA design method, 3D finite element modelling was conducted on a geometric parameter space shown in Table 4 (Byrne et al., 2015) in order to verify the design method. This will be referred to as the PISA project design space.

3.4.1 PISA Soil Stiffness Formulae

As the PISA project is currently ongoing, the derivations of the soil stiffness components and the numerical values of their coefficients are confidential and cannot be presented in this paper. The general formulae for the stiffness components are shown in Table 5.

3.5 DTU 10 Megawatt Reference Wind Turbine (DTU 10MW RWT)

The Technical University of Denmark (DTU) originally created the DTU 10MW RWT to serve as a reference for future rotor design comparisons (Bak et al., 2013). While the objective was to focus on the rotor, a complete wind turbine design was produced in order to fully understand the static and dynamic interactions of the whole structure. The wind turbine was designed for an offshore setting in its consideration of loads, however the proposed tower design by DTU was for an equivalent land based model - this will be referred to as the DTU 10MW land based tower design. No monopile foundation was proposed by DTU. ECN then used the DTU 10MW RWT to create an offshore wind turbine with monopile foundation design for a water depth of 50m to explore the limits of monopile support structures and the limitations of current design methods and modelling, including the *p-y* method (Hermans and Peeringa, 2016). The proposed monopile design by ECN incorporated a conical section in order to reduce wave loads in the splash zones and to account for the increase in

Wind Turbine Parameter	Scaling
Mass m	sf^3
Power p	sf^2
Length L	sf
1st Mass Moment of Inertia I_1	sf^4
2nd Mass Moment of Inertia I_2	sf^5

Table 6: DTU 10MW RWT scaling procedure from the NREL 5MW RWT

Inputs	Outputs
Monopile dimensions (D, L/D, D/t)	Load increments
Nodes and corresponding heights above mudline	Nodal lateral displacements
Soil profile file	Nodal moments
Monopile material properties (E, ν, κ)	
Load (direction and magnitude)	
Soil properties (API only): γ', ϵ_{50} and J	

Table 7: Key OxPile inputs and outputs

bending moment towards the mudline. In order to verify the design, the wind turbine was subjected to a natural frequency check, yield and buckling check, and a fatigue damage check.

3.5.1 Up Scaling Wind Turbines

The DTU 10MW RWT's structural definition was based on a direct up scale from the National Renewable Energy Lab's (NREL) 5MW RWT, another reference wind turbine (Jonkman et al., 2009). A scaling factor (sf) of $\sqrt{10/5}$ was used for the scale up from 5MW to 10MW, which is defined as the square root of the ratio of power outputs. The wind turbine parameters and their scaling factors are shown in Table 6. The final mass of the nacelle and hub was adjusted and scaled from the Vestas V-164 8MW wind turbine.

The up scaling procedure used was based on methods described by Sieros et al. (2012) and uses assumptions of geometrical and aerodynamic similarity (fixed rotor tip speed). Theoretically, the aerodynamic forces on a wind turbine would scale with sf^2 and moments would scale with sf^3, however empirical data shows that the loads are actually under-predicted as moments scale closer to sf^4 (Sieros et al., 2012).

3.6 OxPile

OxPile is a pre-existing MATLAB program written by H.J. Burd, R.A. McAdam and C. Abadie to calculate the response of a wind turbine with a monopile foundation in soil when subject to a lateral

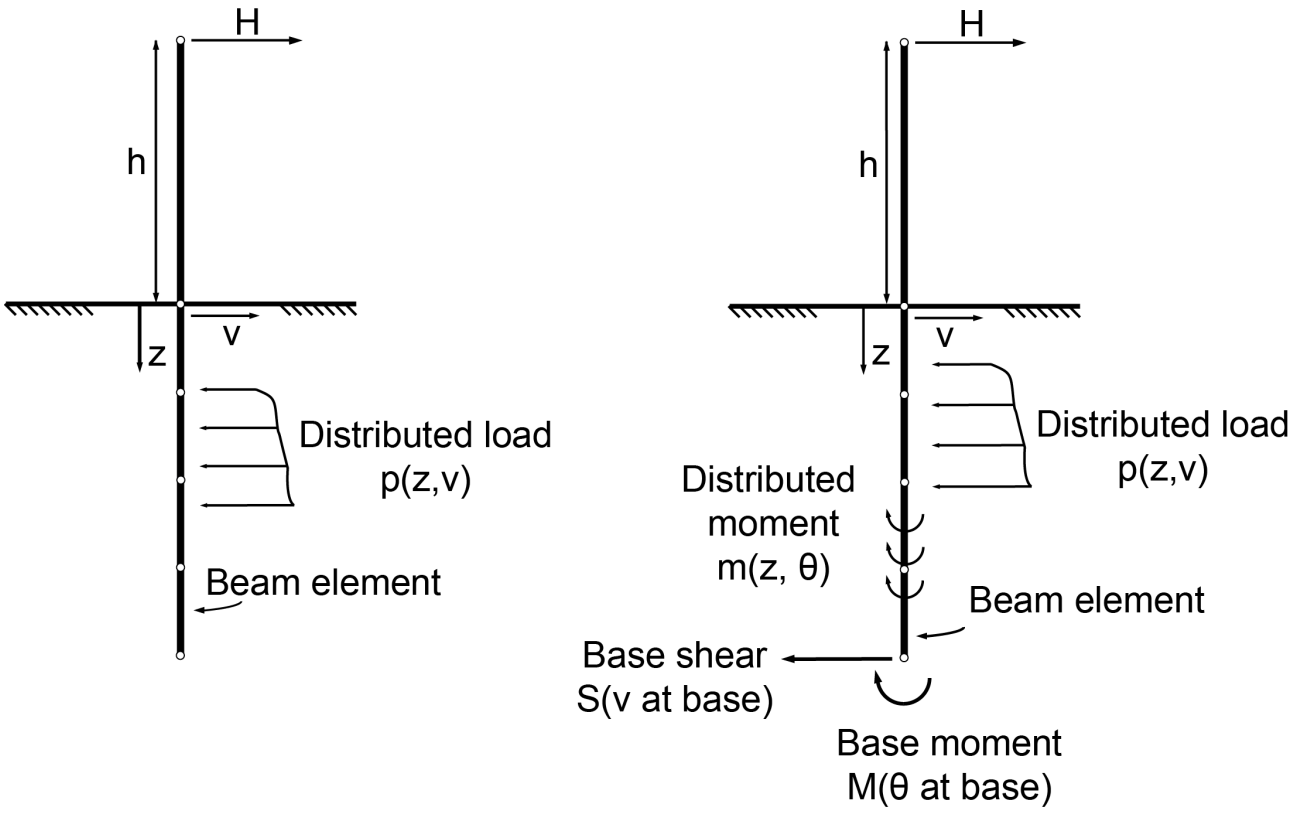

Figure 5: OxPile soil models for API (left) and PISA (right)

loading. OxPile models the wind turbine as a series of 1D finite beam elements and is capable of calculating the static response using both API and PISA soil models. The 1D models used by OxPile can be seen in Figure 5. The wind turbine above mudline is considered a single element whilst the wind turbine below mudline is divided into the remaining desired number of elements. The program applies the design load in constant increments and, using a finite difference method, returns the rotation of the monopile at the mudline for each load increment and the final displacements and moments at each node. The key inputs and outputs of OxPile for a wind turbine are shown in Table 7.

4. Wind Turbine Eigen Analysis

The Eigen Analysis Code (EAC) was developed specially for this project to solve for the natural frequency of a defined wind turbine using eigenvalue analysis of the modelled structure, in order to check if the wind turbine satisfies requirement 3 (natural frequency) of the limit state requirements. A global stiffness matrix, comprising of the soil and beam stiffness elements, and a global mass matrix were generated for the wind turbine's eigen analysis: the EAC was designed to be able to use either the API and PISA method in its calculations. In order to ensure the code's accuracy, verification was conducted through comparison to analytical solutions and mesh refinement was performed.

Inputs
Cross-sectional dimensions and material properties
Number of nodes
Soil profile
Concentrated tower top mass M
Concentrated tower top inertia I
Soil properties (API only): γ', ϵ_{50} and J

Table 8: EAC inputs

4.1 Eigen Analysis Code (EAC)

Height relative to mudline	Diameter	Wall Thickness	Young's Modulus	Density

Table 9: Cross-section dimensions and material properties matrix row

The EAC program returns the fundamental natural frequency of a structure of a given soil profile for the inputs shown in Table 8. The cross-sectional dimensions and material properties input is a matrix with rows consisting of the values shown in Table 9. These are required at every section interface of the wind turbine which are defined as:

- A step change in wall thickness or diameter
- The beginning of a tapered section
- The end of a tapered section
- A change in material properties

Cross-sectional dimensions at nodes within tapered sections are then obtained through interpolation. The EAC models the wind turbine as a series of finite Euler-Bernoulli beam elements with soil reactions acting at nodes below the mudline. The mass of the wind turbine is split into a distributed mass along its length and a point mass and inertia at the tower top; everything up to the end of the tower is modelled as the distributed mass, and everything that is not part of the support structure (nacelle, hub and rotor) is lumped as the point mass.

Figure 6 shows the EAC model and its components; the differences in the components used for the API and PISA methods mentioned in Section 3.4 are presented in Table 10.

4.2 Eigen Analysis

To solve for the natural frequency of the structure, the wind turbine and soil can be modelled as a simple harmonic oscillator. The system can thus be represented by the relationship for a mass-spring

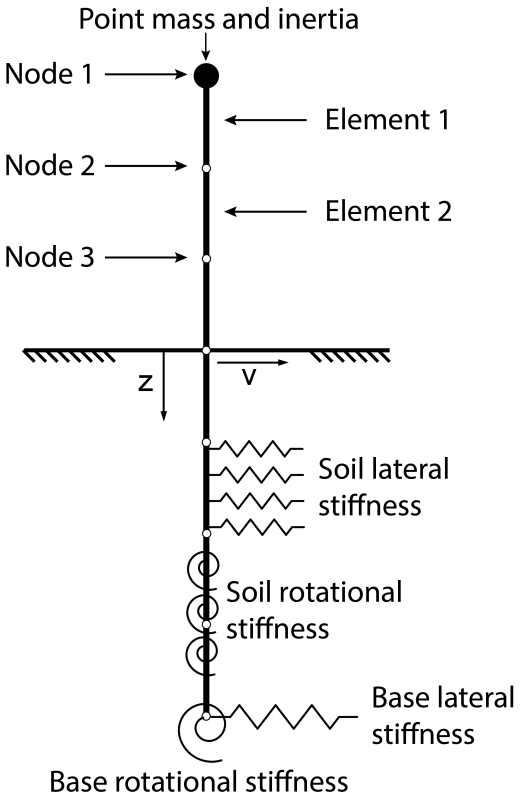

Figure 6: Eigen Analysis Code (EAC) wind turbine model

	Soil lateral stiffness	**Soil rotational stiffness**	**Base lateral stiffness**	**Base rotational stiffness**
PISA	Yes	Yes	Yes	Yes
API	Yes (different formulation)	No	No	No

Table 10: Comparison of PISA and API models used by the EAC

system:

$$\mathbf{M_{global}}\ddot{\mathbf{x}} + \mathbf{K_{global}}\mathbf{x} = 0 \tag{4.1}$$

Where $\mathbf{K_{global}}$ is the global stiffness matrix, $\mathbf{M_{global}}$ is the global mass matrix and $\mathbf{x}$ is the vector of nodal displacements. Rearranging and assuming $\ddot{x} = \omega^2 x$, where ω is the natural frequency, this gives:

$$(\mathbf{K_{global}} - \omega^{\mathbf{2}}\mathbf{M_{global}})\mathbf{x} = 0 \tag{4.2}$$

For which there are only non-zero solutions when:

$$\left|\mathbf{K_{global}} - \omega^{\mathbf{2}}\mathbf{M_{global}}\right| = 0 \tag{4.3}$$

This is the characteristic equation of the system; its eigenvalues are the square of the natural frequencies ω^2, of which the fundamental frequency ω_0 is the value of importance.

4.3 Global Stiffness Matrix

The global stiffness matrix $\mathbf{K_{global}}$ is a $2n_e$-by-$2n_e$ matrix, where n_e is the number of beam elements in the model, as each node has two degrees of freedom; lateral displacement and rotation. The global stiffness matrix consists of the summation of Euler-Bernoulli stiffness elements (due to the beam stiffness) and soil stiffness elements (due to the soil reactions) at their respective nodes in the matrix. Depending on the choice of method, either the API or PISA soil stiffness element will be used.

4.3.1 Euler-Bernoulli Stiffness Element

The stiffness element matrix, for a 2D finite beam element with nodes of 2DOF, is given by Howatson et al. (2009) as:

$$\mathbf{k_{element}} = \frac{EI}{L_e^3}\begin{bmatrix} 12 & 6L_e & -12 & 6L_e \\ 6L_e & 4L_e^2 & -6L_e & 2L_e^2 \\ -12 & -6L_e & 12 & -6L_e \\ 6L_e & 2L_e^2 & -6L_e & 4L_e^2 \end{bmatrix}. \tag{4.4}$$

Where L_e is the element length, E is the Young's modulus, and I is the moment of inertia. These are added into the global stiffness matrix along the diagonal for each element; the value of I is calculated at the mid-point of each element.

4.3.2 API Soil Stiffness Element

From the *p-y* equations shown in Section 3.3.1, an expression for the soil stiffness per unit length of monopile can be expressed as:

$$\frac{dp}{dy} = \frac{k_{soil}}{length} = \frac{p_u}{2y_c}(\frac{1}{0.1})^{\frac{2}{3}} \tag{4.5}$$

The calculation procedure for lateral soil stiffness component in the API soil model for $\mathbf{K_{global}}$ is then:

- Calculate soil stiffness per unit length dp/dy for every element below mudline at their mid-point
- Multiply dp/dy by element length L_e to obtain k_{soil}
- Divide k_{soil} by 2 and add to the end nodes of the corresponding element in $\mathbf{K_{global}}$

The result is an additional soil stiffness component at all $\mathbf{K_{global,ii}}$ odd terms that correspond to nodes below mudline.

4.3.3 PISA Soil Stiffness Element

Using the formulae described in Section 3.4 for PISA soil stiffness, the procedure for solving for the lateral and rotational PISA soil stiffness is:

1. Calculate lateral and rotational soil stiffness per unit length monopile, dp/dv and $dm/d\psi$, for every element below mudline at their mid-point
2. Multiply dp/dv and $dm/d\psi$ by element length L_e to obtain $k_{soil,v}$ and $k_{soil,\psi}$
3. Divide $k_{soil,v}$ and $k_{soil,\psi}$ by 2 and add to the corresponding elements two nodes in $\mathbf{K_{global}}$

The result is an additional term at all $\mathbf{K_{global,ii}}$ odd terms below mudline due to $k_{soil,v}$, and an additional term at all $\mathbf{K_{global,ii}}$ even terms due to $k_{soil,\psi}$. The base shear stiffness and base rotational stiffness are calculated and simply added to the penultimate and last diagonal element of $\mathbf{K_{global}}$ respectively.

4.4 Global Mass Matrix

The global mass matrix $\mathbf{M_{global}}$ is a $2n_e$-by-$2n_e$ matrix; the same size as $\mathbf{K_{global}}$. The elements are assembled in the same way through adding into the matrix at the corresponding node locations.

4.4.1 Mass Element Matrix

The element mass matrix for Euler beams is defined by Burd (2017) as:

$$\mathbf{m_b} = \frac{\rho A L_e}{420}\begin{bmatrix} 156 & 22L_e & 54 & -13L_e \\ 22L_e & 4L_e^2 & 13L_e & -3L_e^2 \\ 54 & 13L_e & 156 & -22L_e \\ -13L_e & -3L_e^2 & -22L_e & 4L_e^2 \end{bmatrix} + \frac{\rho I}{30L_e}\begin{bmatrix} 36 & 3L_e & -36 & 3L_e \\ 3L_e & 4L_e^2 & -3L_e & -L_e^2 \\ -36 & -3L_e & -36 & -3L_e \\ 3L_e & -L_e^2 & -3L_e & 4L_e^2 \end{bmatrix} \tag{4.6}$$

This is added into $\mathbf{M_{global}}$ at the corresponding matrix locations for each element.

4.4.2 Tower Top Mass and Inertia

The nacelle, hub, and rotor blades are modelled as a point mass and inertia. The point mass and point inertia are added into $\mathbf{M_{global}}$ at the first and second diagonal element respectively.

4.5 Code Verification

The components of the EAC were verified in two stages:

- Stage 1: Euller-Bernoulli beam stiffness elements (in $\mathbf{K_{global}}$) and global mass matrix $\mathbf{M_{global}}$ verification
- Stage 2: global stiffness matrix $\mathbf{K_{global}}$ (both beam and soil stiffness elements) verification

The beam stiffness elements and the global mass matrix (stage 1) were verified by running the EAC for various simulated cantilever scenarios for which analytical solutions exist. The global stiffness matrix (stage 2) was verified by comparing the displacements calculated by the EAC to those of OxPile for piles with a lateral end load.

4.5.1 Beam Stiffness Elements and Global Mass Matrix Verification

Test Tower	**Wall Thickness (m)** t	**Diameter (m)** D	**Height (m)** h
1	0.059	5.9	39
2	0.104	7.04	69
3	0.149	9.9	99

Table 11: Code verification test towers

Stage 1 of the verification (various cantilever scenarios) used three test towers, shown in Table 11, with a mesh of 200 nodes; the towers are open-ended cylinders, the same shape as monopiles. The dimensions were chosen as arbitrary, non-whole number values in order to avoid any false positive results; they were not chosen to represent a geometric design space.

A vertical cantilever was simulated by setting $L = 0$ and removing the soil stiffness elements from the EAC. Then, the rotational and lateral stiffness of the mudline node in the global stiffness matrix was multiplied by a large factor K to simulate a fixed end; a finite value was required as a precaution against numerical errors in MATLAB, whereas theoretically it would be infinite. A value of K was obtained by applying a lateral end load of 999N on the three test towers; plots of natural frequency (ω) against K and end deflection (δ_e) against K showed that ω and δ_e had converged to their respective limits by approximately K = 10^{17}, so this value was used for the verification.

Using the EAC, the test towers were simulated as cantilevers in each of the the three scenarios shown in Figure 7 to verify the beam stiffness elements in $\mathbf{K_{global}}$ and the global mass matrix $\mathbf{M_{global}}$. The results are shown in Table 12. It can be seen that the maximum error for scenario 3 is considerably higher than those for scenarios 1 and 2; this is because the analytical solution does not consider rotational inertia terms whereas the mass matrix given by Burd (2017) does. As the cantilever becomes more slender, the inertial terms become less significant and the error reduces considerably, in line with scenarios 1 and 2.

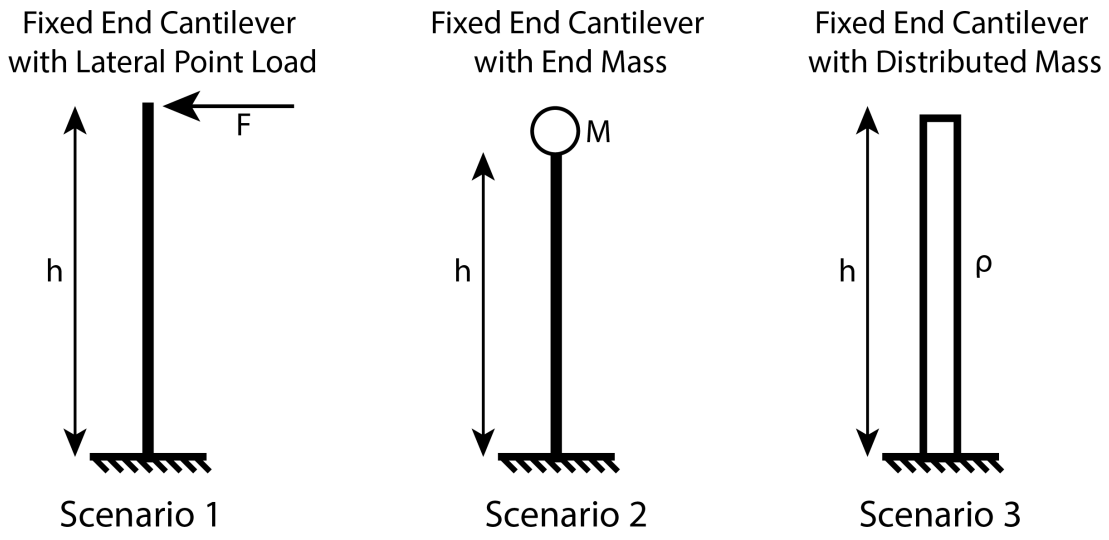

Figure 7: Fixed end cantilever scenarios simulated by the EAC for code verification

Scenario	Additional Parameters	Analytical Solution	Maximum Error
1	F = 999N	$\delta_e = \frac{Fh^3}{3EI}$	0.057%
2	M = 999kg	$\omega = \sqrt{\frac{3EI}{Mh^3}}$	0.012%
3	ρ = 999kg/m^3	$\omega = 1.875^2\sqrt{\frac{EI}{\rho Ah^4}}$	1.1%

Table 12: Code verification results for fixed end cantilever scenarios

4.5.2 Soil Stiffness Verification

Stage 2 of the verification (comparing the EAC's results to OxPile's) used three test piles, shown in Table 13, with the same dimensions and shape as the three previous test towers except now with embedded lengths; a mesh of 200 nodes was used again. The focus of stage 2 was to ensure the soil stiffness calculations were accurate for both API and PISA methods.

Preliminary verification was conducted on the test piles by multiplying the soil stiffness elements in $\mathbf{K_{global}}$ by a factor K_2; a range of K_2 values from 10 to 10^{10} resulted in monotonically increasing values of ω_0 as expected.

Following this, the nodal displacements predicted by the EAC and OxPile when the test piles were subject to a lateral end load of 99.999kN, in API and PISA soil models, were compared. The stiffness matrix produced by the EAC was used to solve for the nodal displacements by inverting Hookes law in matrix form: $\mathbf{x} = \mathbf{K_{global}}^{-1}\mathbf{F}$, where $\mathbf{x}$ is the vector of nodal displacements and $\mathbf{F}$ is the vector of nodal forces. Vector $\mathbf{x}$ was compared to the displacements predicted by OxPile; Figure 8 shows the plots of nodal deflections for test pile 3 using the PISA model soil reactions. Above mudline, the wind turbine displacement was only sampled at the end point by OxPile, thus the predicted above

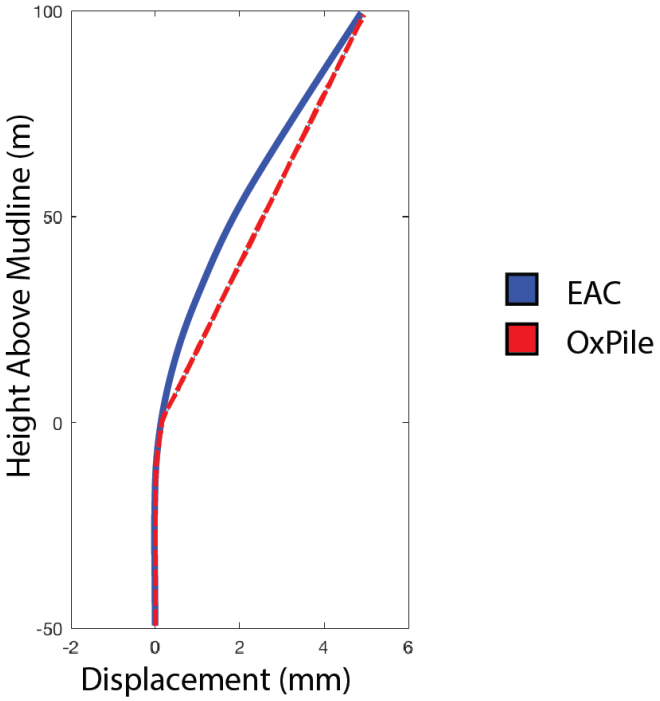

Figure 8: Nodal displacements calculated by the EAC (blue) and OxPile (red) with PISA method soil reactions for test pile 3 (99.999kN lateral end load)

Test Pile	**Wall Thickness (m)** t	**Diameter (m)** D	**Height (m)** h	**Embedded Length (m)** L
1	0.059	5.9	39	29
2	0.104	7.04	69	39
3	0.149	9.9	99	49

Table 13: Code verification test piles

mudline displacement only matched the EAC's at the top of the pile. For the three test piles and for both API and PISA methods, a maximum error of $< 3\%$ was found at mudline. The larger maximum error compared to the scenarios of stage 1 is due to the different way the EAC and OxPile applies the soil reactions to the monopile; the EAC lumps the soil reactions into lateral forces at nodes, whereas OxPile distributes the forces, resulting in additional moments.

4.6 Mesh Refinement

In order for the EAC to accurately model a continuous wind turbine with a finite number of nodes, the placement of the nodes had to be optimised. Additionally, an estimation of the number of nodes required for the natural frequency to fall within an acceptable tolerance of the true natural frequency was necessary.

4.6.1 Node Placement

The stiffness and mass elements of the wind turbine and soil stiffness elements were calculated at the mid-point of every element, then split and distributed to the element's end nodes. Thus, to obtain an accurate model, the EAC ensures the following:

1. There is always a mudline node, so that soil reactions are calculated for the exact length of monopile below the mudline
2. A node falls on every section interface (as described in Section 4.1) so that the EAC does not incorrectly interpolate within elements of straight and tapered sections or elements with nodes of different wall thicknesses and densities
3. The desired number of nodes are distributed as evenly as possible within each section and along the structure, ensuring regular sampling of soil stiffness, beam stiffness, and mass along the length of the wind turbine

4.6.2 Minimum Number of Nodes

It is not possible to obtain an analytical solution of the natural frequency of a beam with straight and tapered sections. Thus, the true natural frequency for the wind turbine was considered to be the natural frequency as the number of nodes became very large, as it effectively becomes close to a continuous model. The assumed true natural frequency is supported through verification of the EAC in Section 4.5. A mesh of 300 nodes was chosen to represent the true natural frequency. Analysis of monopile combinations in the PISA project design space with the DTU 10MW land based tower design, using the Cowden Till soil profile, fell within 1% of the true natural frequency within approximately 50-75 nodes for both API and PISA soil models. Therefore, a minimum number of 100 nodes for modelling a wind turbine was chosen to be conservative. Graphs of the natural frequency against number of nodes for the API and PISA methods are shown in Figure 9, for D = 10, t = 0.1 and L = 30 and with the DTU 10MW land based tower design.

5. Wind Turbine Static and Combined Analysis

To complete the analysis of a given wind turbine, the Static Analysis Code (SAC) was developed for this project to check if a given monopile satisfies the limit state requirements 1 (yield) and 2 (displacement), detailed in Section 3.2. The SAC makes use of the OxPile program. Finally, a Combined Analysis Code (CAC) was written to combine the SAC and EAC, and to be able to apply them efficiently to a given geoemtric parameter space.

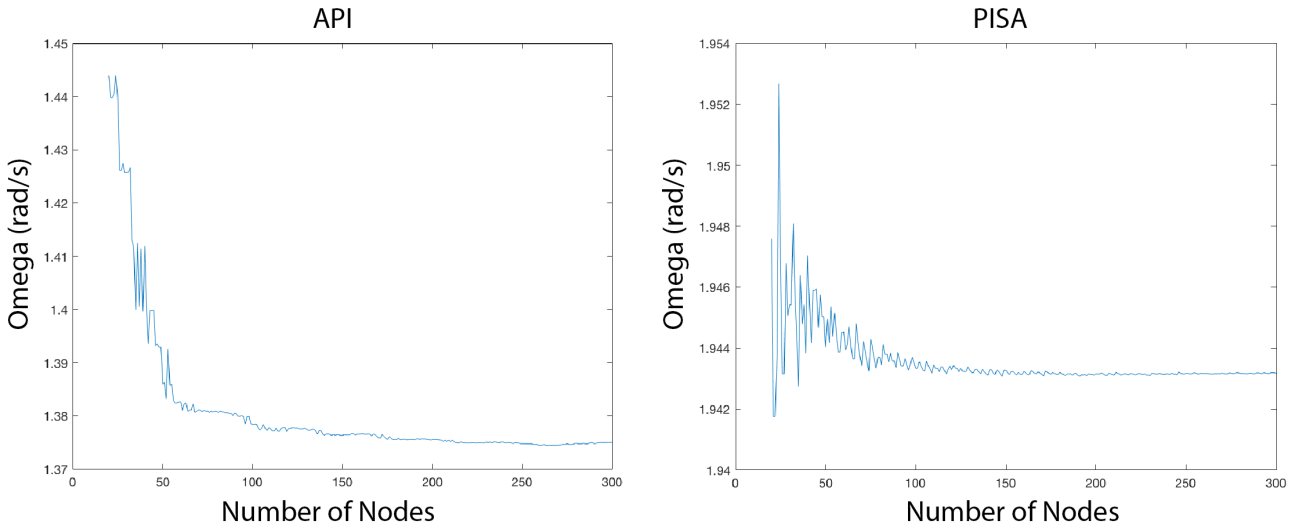

Figure 9: Plots of omega against number of nodes for API (left) and PISA (right)

5.1 Static Analysis Code (SAC)

The SAC uses OxPile, described in Section 3.6, to model the monopile and to calculate its static response to a lateral load. The outputs of OxPile are then analysed to check if the monopile has satisfied the ULS requirements.

5.1.1 Requirement 1: Yield Check

The SAC assumes the monopile behaves as a beam under simple bending and thus expresses the maximum bending stress as:

$$\sigma_{max} = \frac{MD}{2I_x} \tag{5.1}$$

Where M is the section moment, I_x is the section second moment of area of the monopile, and D is the pile diameter. The SAC checks for yield by solving for the bending stress at each node using the nodal moments predicted by OxPile and comparing it to the design yield strength of the steel.

5.1.2 Requirement 2: Mudline Displacement Check

The SAC checks Requirement 2 by comparing the maximum allowable deflection (which will be defined in Section 6.1) to the mudline node displacement returned by OxPile.

5.2 Combined Analysis Code (CAC)

The CAC combines the SAC and EAC, and analyses combinations of monopile parameters within a defined D - (L/D) - (D/t) parameter space, e.g. the PISA project design space. The CAC inputs and outputs are shown in Table 14. The code works as follows:

Inputs	Outputs
D range	SAC pass/fail record for every combination analysed
L/D range	Natural frequency for every combination analysed
D/t range	
PISA/API	
Optimum natural frequency range	
Number of points	
Tower design	

Table 14: Combined Analysis Code (CAC) inputs and outputs

1. Select equally spaced values within each parameter range depending on 'number of points' input
2. For a combination of monopile parameters (a sample), use the SAC to check if the limit state requirements are satisfied
3. Record if the SAC checks are passed and, if not, which have failed
4. For the same combination, use the EAC to calculate and record the natural frequency of the whole wind turbine
5. Repeat for all other combinations

The result is a parameter space of equally distributed samples, with the recorded natural frequency and the SAC pass/fail record for each sample.

6. Design Scenario

The design scenario described in Section 2.2 was defined fully first for a water depth of 30m and 10MW wind turbine in order to provide a basis for the subsequent modelling, and scenarios of increasing mean water level and wind turbine power rating.

6.1 Limit State Requirements

Table 15 shows the exact values for the three limit state requirements described in Table 3. Requirement 1 was obtained from the European Standard EN 10025-2 and the values are detailed in Section 6.3. Requirement 2 was obtained from PISA which used a maximum deflection of $D/10$ as a criterion for ultimate failure; while this value is conventionally adopted, Byrne et al. (2017) noted that there is no rigorous basis for its use as a defining value. The value of optimum natural frequency for requirement 3 was calculated as the midpoint between the 1P and 3P ranges; the minimum and maximum rotor speeds are given as 6rpm and 9.6rpm respectively by DTU. Figure 10 shows a visualisation of the 1P and 3P frequency ranges for the 10MW wind turbine. It was decided that a tolerance of $\pm 5\%$ of the value of optimum natural frequency was considered acceptable for requirement 3.

Requirement	Type	Values	Source
1 (yield)	ULS	Shown in Section 6.3	European Standard EN 10025-2
2 (displacement)	ULS	$0.1D$	PISA (Byrne et al., 2017)
3 (natural frequency)	FLS	1.4451 rad/s $\pm 5\%$	DTU (Bak et al., 2013)

Table 15: Limit state requirements for the design scenario

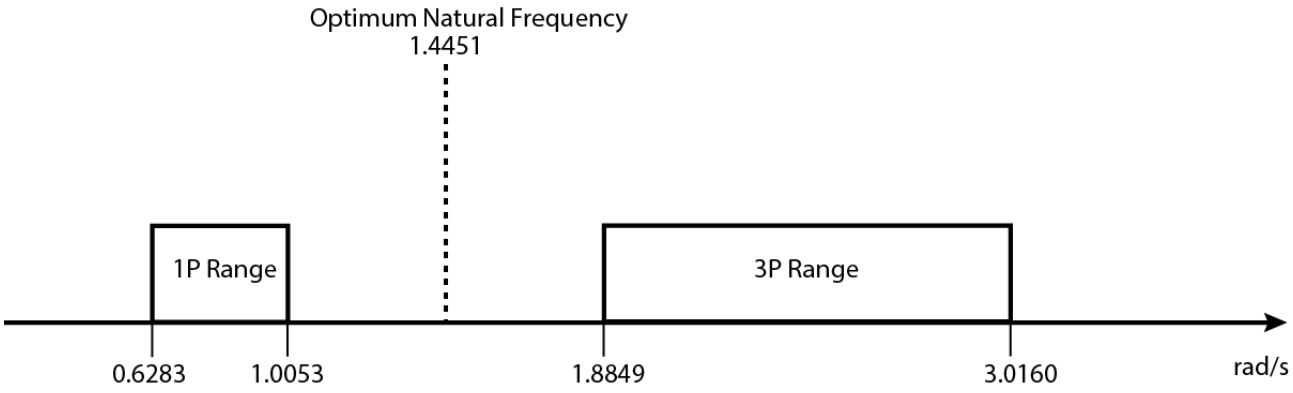

Figure 10: Visualisation of 1P and 3P ranges for the 10MW wind turbine

6.2 Loads

The ultimate wind loads for the 10MW RWT were produced by DTU and subsequently revised by ECN. DTU determined the extreme load case for the wind turbine using Design Load Case 1.3, using statistical extrapolation recommended by Germanischer Lloyd (2010); this is given as a 4605kN (including partial factors) lateral point force at the tower top which is a result of extreme conditions during operation. This value was revised by ECN after modelling the wind turbine with aero-elastic code and considering 828 load cases. The new value of ultimate load was determined to be 3265kN (including partial factors). This value obtained by ECN was used for the design process.

Hydrodynamic loading was not considered in the DTU paper. ECN estimated the hydrodynamic loading using the Upwind Cost Model (de Vries, 2011) where the Morison equation is used to obtain a first estimate of extreme loads. However, ECN states that it is overly conservative to consider both wave and operational wind ultimate loads simultaneously as a wind turbine would not be operational during periods of extreme weather. As a result, no hydrodynamic loading is considered as it is small in comparison to the ultimate wind load.

As mentioned previously in Section 6.1, cyclic loading was not directly considered in this project.

6.3 Material Specifications

The wind turbine design uses S355 steel, which is that used by the DTU 10MW RWT. The material properties are obtained from the European Standard EN 10025-2 and are shown in Table 16. It

Property	Value	Unit
Young's Modulus E	210	GPa
Poisson's Ratio ν	0.3	-
Density (monopile) ρ	7855	kg/m^3
Density (tower) ρ	8500	kg/m^3

Table 16: Wind turbine material properties

Thickness (mm)	Characteristic Yield Strength (MPa)
t $\leq$ **16**	355
16 $<$ **t** $\leq$ **40**	345
40 $<$ **t** $\leq$ **63**	335
63 $<$ **t** $\leq$ **80**	325
80 $<$ **t** $\leq$ **100**	315
100 $<$ **t** $\leq$ **150**	295
150 $<$ **t** $\leq$ **200**	285

Table 17: S355 steel yield strength with varying thickness

should be noted that the density of the tower steel has been increased to 8500 kg/m^3 to account for the mass of secondary structures, such as accessibility features, cables, and joints, as recommended by DTU.

The S355 steel used in the design of the wind turbine would require hot rolling for manufacture. This produces different values of yield strength depending on the final thickness of the steel; thinner sections require more working, resulting in an increase of yield strength. The values are again obtained from EN 10025-2 and are shown in Table 17.

6.4 Soil Profile

The soil profile of the Cowden site was used (Cowden Till soil profile), as it was determined during the PISA project to be representative of a North sea overconsolidated clay profile, typical to several wind farms (Byrne et al., 2015). The soil parameters used are shown in Table 18 and the variation of undrained shear strength s_u and small strain, non-linear tangent shear modulus G_0 with depth are shown in Figure 11.

6.5 Sea Level

In order to compare the design methods of PISA and API, a mean water level of 30m was chosen as the smallest water depth, as wind turbines have already been designed for that depth. It was decided that an extreme sea state single wave amplitude of 15m would be used, similar to the NREL

Property	Value	Unit
Effective Unit Weight γ'	11000	kN/m^3
Poisson's Ratio ν	0.3	-
Empirical Constant J	0.5	-
Strain at 50% Ultimate Load from Triaxial Test ϵ_{50}	0.0115	-

Table 18: Soil parameters for design scenario

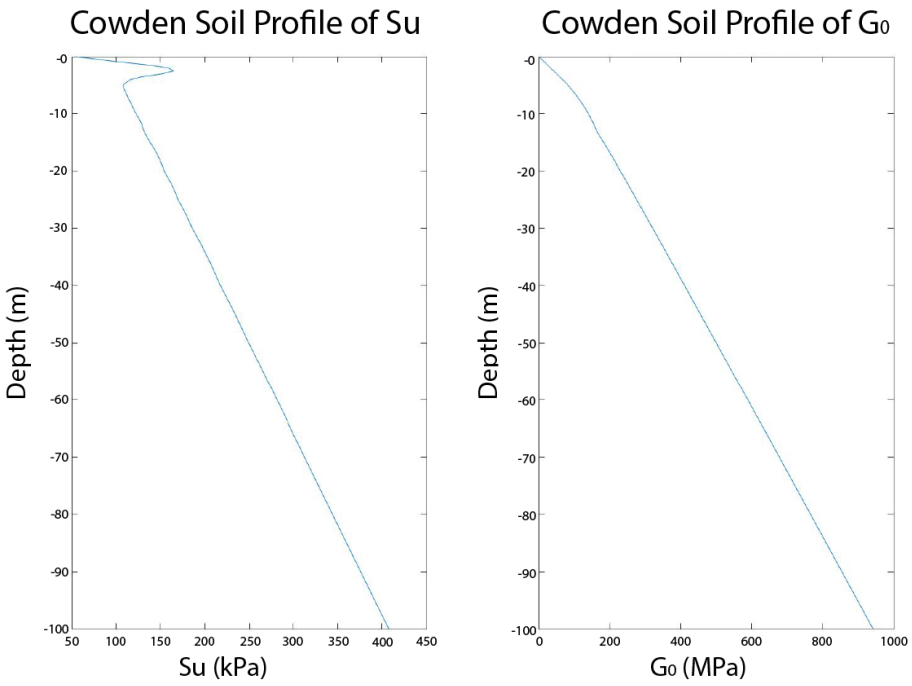

Figure 11: The Cowden Till soil profile of s_u (left) and G_0 (right)

5MW RWT scenario (Jonkman et al., 2009), so that realistic sea conditions would be considered in the design.

6.6 Safety Factors

It was necessary to employ safety factors for the design of the wind turbines to produce realistic designs. Safety factors were used for the steel strength, soil parameters, and the ultimate load in the ULS calculations by the SAC. The EAC does not use safety factors in order to get the most accurate value of natural frequency of the wind turbine.

6.6.1 Steel Parameters

It is assumed that, if the steel yields, it will do so through tensile fracture. AD 388 (NSC, 2015) recommends a safety factor of 1.25 for tensile fracture. The design yield strength can then be calculated using the characteristic steel properties:

$$\sigma_{yd} = \frac{\sigma_{yk}}{1.25} \tag{6.1}$$

6.6.2 Soil Parameters

The values given in the Cowden Till soil profile are best estimates of the soil parameters taken from empirical testing. The best estimate of G_0 was used without safety factors, but it was necessary to determine a design undrained shear strength (s_{ud}) for the static analysis. The characteristic undrained shear strength (s_{uk}) can be calculated, above which 95% of tests will be expected to fall, as $s_{uk} = s_u(1 - (1.65 \times s.d.))$, where $s.d.$ is the standard deviation of the best estimate. The design undrained shear strength can then be calculated from the characteristic shear strength as $s_{ud} = \frac{s_{uk}}{\gamma}$, where γ is the partial safety factor. However, the standard deviation of the undrained shear strength is not known, so an estimate of 10% was used. A partial safety factor of 1.25 was then chosen as conservative estimate for s_u. The design undrained shear strength was thus calculated as:

$$s_{ud} = \frac{s_u(1 - (1.65 \times 0.1))}{1.25} \tag{6.2}$$

6.6.3 Ultimate Wind Load

The safety factor used for the ultimate operational wind load in extreme weather was 1.35, which is recommended by ECN.

7. Design Process

In this Section, the design process of a 10MW wind turbine in 30m depth for the design scenario is described; a single tower design was used for both API and PISA methods. Both API and PISA method monopile geometries were selected within a geometric parameter space (which will be referred to as the design space), which is based on the PISA project design space (Table 4), in order to provide a realistic comparison as the PISA method has not been verified outside of the space. The monopile geometries were chosen to be as cost-efficient as possible, i.e. the cheapest. The final results and the data collected during the design process were analysed to develop understanding of the design space. For this project, the simplified design process for the wind turbine consists of two stages with a feedback loop:

- Stage 1: Tower Design
- Stage 2: Monopile Design

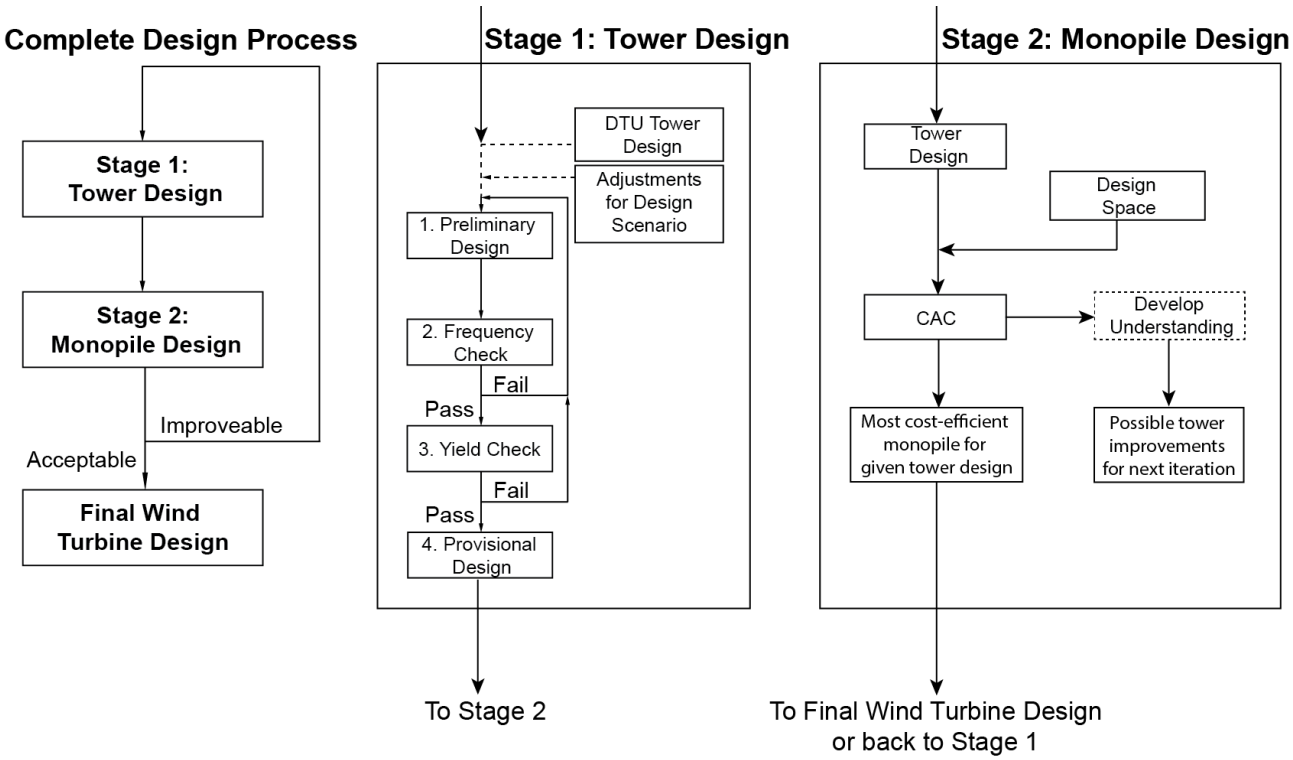

Figure 12: Wind turbine design process flow charts

Figure 12 shows the complete design process flow chart for the wind turbine as well as the breakdown of the individual design stages. As the tower and monopile interact to create a combined natural frequency for the structure, the feedback loop in the complete design process is required as each part cannot be designed independently of the other.

7.1 Monopile Cost-Efficiency

In line with the motivations for the project, the monopiles were designed to be as cost-efficient as possible; the main costs of monopile foundations are typically the installation (driving of the monopile into the ground) followed by the material (Junginger and Faaij, 2004). Thus, the most cost-efficient design can be approximated to the monopile of minimum length followed by minimum mass. It should be noted that the exact costing for construction of a theoretical wind turbine is not possible due to the amount of variables involved, therefore an exact measure of cost-efficiency cannot be obtained. The algorithm used in this project for measuring cost-efficiency rewards any reduction in embedded length regardless of the accompanying increment in mass. This is clearly unrealistic as the price of a monopile will not vary linearly with increase in a geometric parameter; it will depend strongly on the manufacturing, transportation and installation capabilities available, e.g. a reduction of D might have greater cost savings than a reduction of L at $D = 10$m. Noting these limitations, the algorithm described is used as an estimation of cost-efficiency.

7.2 Tower Design

For this project, the tower design was developed so that a reasonable range of monopiles would satisfy the limit state requirements. In practice, a single tower design would be produced for an entire wind farm and the monopile designer may not have the ability to alter it.

The tower design was prioritised first in the design process, as operational requirements must always be met, making its design less flexible than the monopile's. As can be seen in Figure 12, a preliminary design was first created that met the operational requirements of the wind turbine. Following this, a series of checks were run; alterations were made to the key tower parameters until the the checks were passed. Finally, the viable tower design was passed through to Stage 2: monopile design. It should be noted that tower design is out of the scope of this project. As a result, the transition piece was not considered.

7.2.1 Preliminary Design

The DTU 10MW RWT land based tower was used as a starting point for the preliminary design and adjustments were then made to adapt the original land based design for the new 30m mean sea level scenario; the tower top height and tower starting height were raised 30m and 45m respectively from mudline, resulting in a shortening of the tower length by 15m. The adjustments were made to ensure that:

1. The blade clearance from maximum sea level remained the same as DTU's blade clearance from ground level
2. The tower top height relative to mean sea level would be the same as the DTU's tower top height relative to ground level, so that the estimated wind loads remain accurate
3. In extreme sea states, waves do not hit the tower

The tower top mass is defined by DTU as 674,002kg with no inertia; this value was used for the wind turbine as a point mass.

7.2.2 Frequency Check

The preliminary design was then combined with a very stiff monopile and very soft monopile (that lay within the PISA project design space) in order to ascertain a rough frequency range of the overall wind turbine. The goal was to obtain a natural frequency that centred approximately above the optimal frequency of 1.4451 rad/s; the API method soil reactions were used for the calculation. Using the feedback loop of the tower design flow chart, the tower's stiffness was altered until this was satisfied through adjustment of the wall thickness, diameter, taper and length of tower sections. Tower designs of other offshore wind turbines were used as guidelines.

Height above Mudline (m)	Outer Diameter (m)	Wall Thickness (mm)
45	7.5	80
85	7.5	80
122	6	80
122.001	6	20
145.63	5.5	20

Table 19: Tower dimensions at section interfaces

7.2.3 Yield Check

A yield check was applied on the tower using the same method for the monopile yield check. Yield was found not to be a limiting factor and so no alterations were made.

7.2.4 Provisional Design

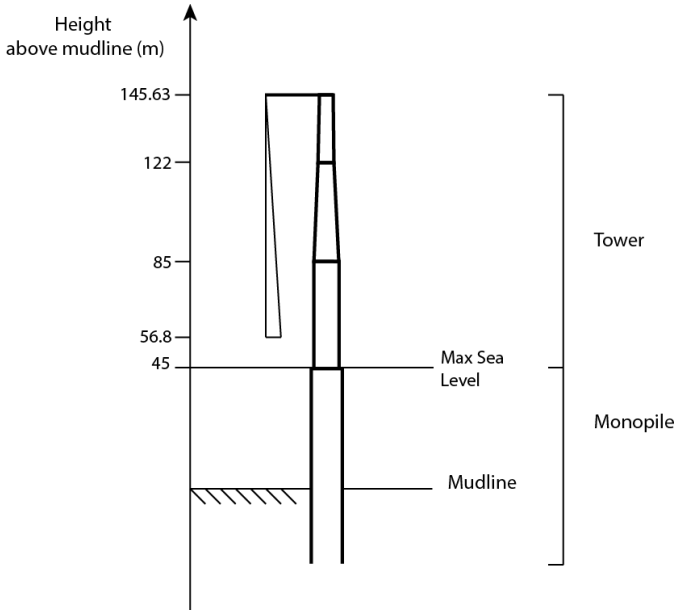

Figure 13: Provisional tower design

The provisional design is shown in Figure 13 and the dimensions at the section interfaces are given in Table 19; note the heights are given in metres above mudline.

7.3 Monopile Design

Stage 2 of the design process was conducted by using the Combined Analysis Code (CAC) to find the most cost-efficient monopile with the previously designed tower. The data obtained from the CAC was then used to develop an understanding of the main limiting factors of monopile efficiency and to suggest improvements for the next iteration of the design process.

Using the designed tower from Stage 1, the natural frequencies and pass/fail records of combinations

Parameter	Range
Diameter D (m)	7.5-10
Aspect Ratio L/D	2-6
Thickness Ratio D/t	60-110

Table 20: Design space for the 10MW wind turbine, 30m depth (adjusted from PISA project design space)

Requirement	Type	Values
1 (yield)	ULS	Shown in Section 6.3
2 (displacement)	ULS	0.1D
3 (natural frequency)	FLS	1.4451 rad/s $\pm 5\%$

Table 21: Limit state requirements for the design scenario

of monopile dimensions within the geometric parameter space (design space) were obtained for the PISA and API methods. The design space explored was adjusted from the PISA project design space; the diameter range was updated to 7.5m to 10m as the monopile cannot have a diameter smaller than the base of the tower. The explored design space is shown in Table 20.

7.4 Results

The limit state requirements for the project are shown again in Table 21 for cross-referencing with the results and analysis.

7.4.1 Most Cost-Efficient Monopile Geometries

The most cost-efficient monopile geometries, as described in Section 7.1, determined by the CAC are shown in Table 22; the mass shown is that of the monopile below mudline. These were obtained using $20 \times 20 \times 20$ samples of monopile dimension combinations within the adjusted PISA design space shown in Table 20.

7.4.2 Natural Frequency Surfaces

Using the data collected by the CAC, 3D surfaces showing the natural frequency of the 10MW wind turbine against L/D and D/t were plotted for different diameters within the design space in

Method	D (m)	L (m)	t (mm)	L/D	D/t	Mass (kg)
API	10	30.53	130	3.05	76.9	966,680
PISA	8.04	23.27	70	2.89	114.9	320,370

Table 22: Most cost-efficient monopile geometries for the API and PISA methods

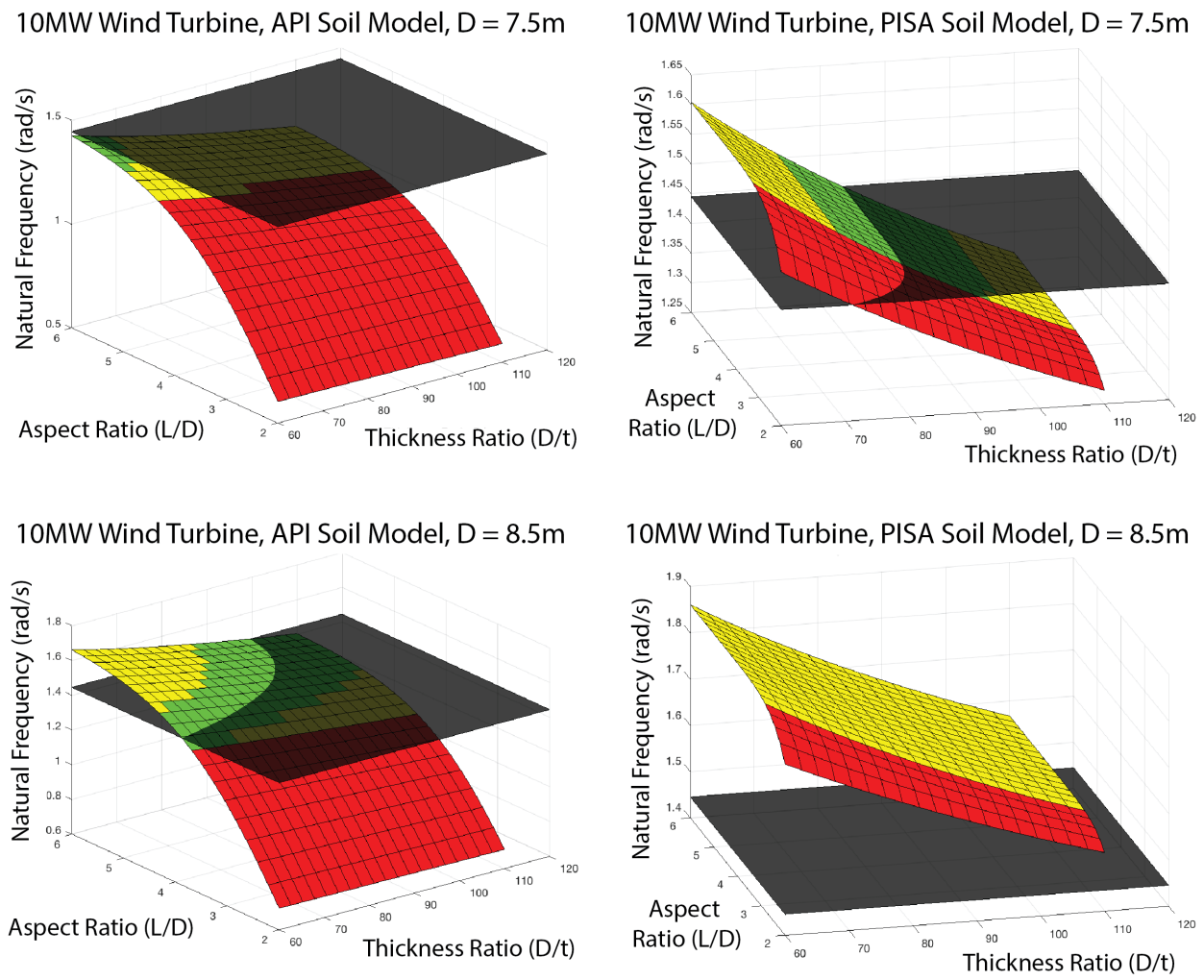

Figure 14: Surfaces of wind turbine natural frequency against L/D and D/t for diameters 7.5m and 8.5m (10MW, 30m depth); the black planes represent the optimum natural frequency; red areas show combinations that fail a ULS requirement, yellow areas show combinations that only fail FLS requirement 3, and green areas show combinations that satisfy all three requirements

order to develop understanding as part of the design process. The results for monopiles of diameters 7.5m and 8.5m are shown in Figure 14. The black plane in each plot represents the optimum natural frequency and is referred to as the 'optimum natural frequency plane': the surface of natural frequency is referred to as the 'monopile surface'. Areas are colored red if they fail either of ULS requirements 1 and 2, yellow if they pass both ULS requirements but not FLS requirement 3, and green if they pass all three requirements. The data collected by the CAC showed that, of the two ULS requirements, only requirement 2 is failed in the explored design space; yield is never a limiting factor.

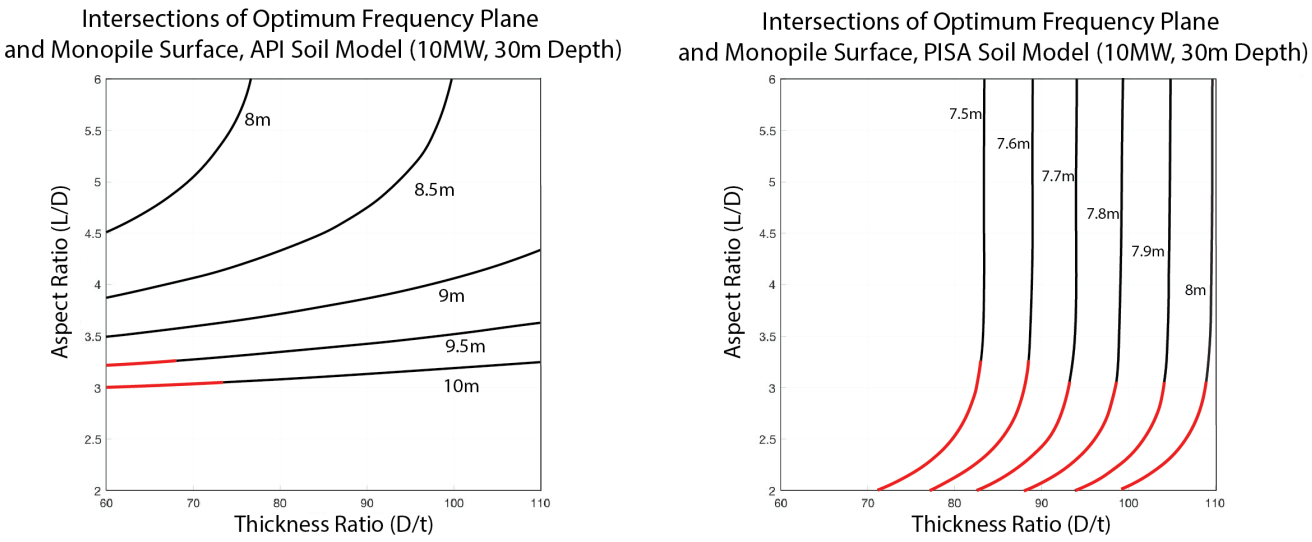

Figure 15: API (left) and PISA (right) 2D interaction curves (10MW, 30m Depth); curves show the intersections of optimum frequency plane and monopile surface for different diameters; black lines show combinations that satisfy all three requirements and red lines show combinations that fail a ULS requirement

7.4.3 2D Interaction Curves

2D 'interaction curves' were then plotted showing the intersection of the monopile surfaces and the optimum frequency planes (i.e monopile parameter combinations that satisfy FLS requirement 3 at 1.4451rad/s as calculated by the CAC); these are shown in Figure 15. Black lines show parameter combinations that pass all three requirements and red lines show combinations that fail a ULS requirement (which was found to be only requirement 2). The 2D interaction curves aim to show the FLS constraint on the available choice of monopile parameters.

7.4.4 ULS Plots

Figure 14 shows that the monopile parameter combinations that fail ULS requirements are bounded by lines of constant L/D; the line for each diameter will be referred to as the 'ULS line'. 2D plots of these bounds are shown in Figure 16; the space above the ULS lines in L/D - D/t space are parameter combinations that satisfy the ULS requirements (for that diameter); the red and black lines represent sections above and under the optimum frequency plane respectively on the ULS lines. The plots aim to show the ULS constraints on the available choice of monopile parameters; i.e. the ULS line shows, for a given diameter, the minimum possible L/D that satisfies the ULS requirements.

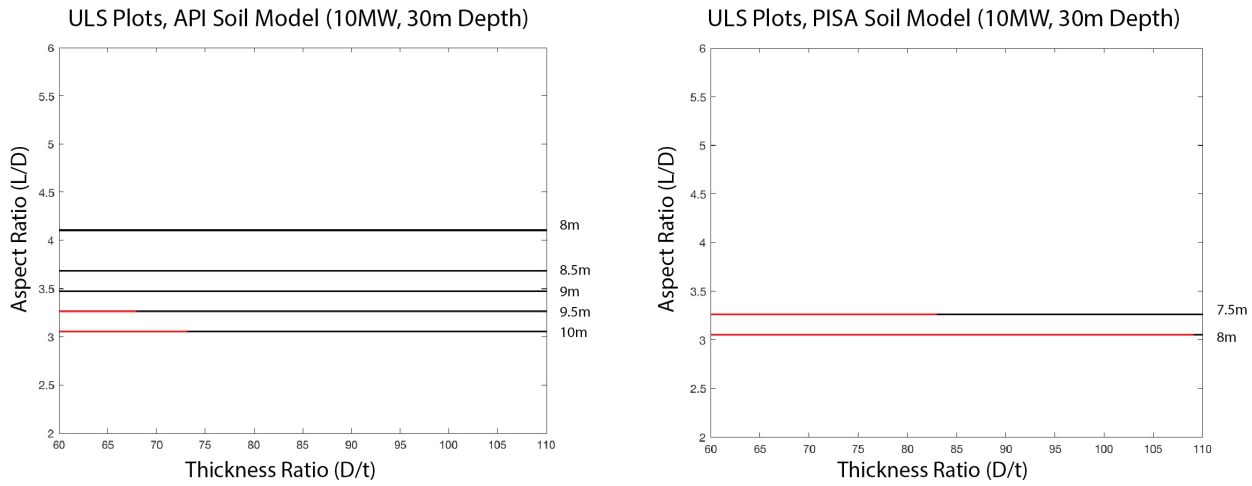

Figure 16: API (left) and PISA (right) ULS plots (10MW, 30m Depth); the area above the lines in L/D - D/t space are combinations that satisfy the ULS requirements for that diameter; the red and black lines represent sections above and under the optimum frequency plane respectively on the bounding line

7.5 Analysis

Analysis was conducted on the individual sets of API and PISA results along with a final comparison.

7.5.1 API Results Analysis

From the natural frequency surfaces in Figure 14, it can be seen that the API method's monopile surface is relatively invariant with D/t at low values of L/D and more variant with D/t at high values of L/D; the peak natural frequency occurs at the combination of maximum L/D and minimum D/t for a given diameter, but changing D/t at low values of L/D does not have a significant effect. Increasing L/D also results in an increase of natural frequency, however the natural frequency appears to be reaching a limit at the largest values of L/D. The natural frequency surfaces also show (by comparing diameters 7.5m to 8.5m) that an increase of diameter results in a general translation of the whole monopile surface upwards in the frequency axis, which is expected; a larger diameter would increase both the second moment of area of the monopile and also the magnitude of the soil reactions (as they scale with D), thus increasing the stiffness of the structure.

The API method 2D interaction curves (Figure 15) highlight how the combinations of monopile parameters required for the wind turbine to meet the optimum natural frequency change as individual parameters are varied. The inconsistent shapes of the curves as diameter increases are a result of

the changing relationship between natural frequency and D/t as L/D increases; D/t has relatively little effect on the natural frequency at low values of L/D. Thus the viable monopile parameter combinations that satisfy the FLS requirement for a given diameter depend strongly on where the optimum natural frequency intersects the monopile surface in Figure 14. Comparing the various diameter monopiles in the interaction curves (Figure 15), larger diameters are able to have smaller values of L/D as they would provide more stiffness through a combination of larger soil reactions and greater second moment of area (as they both scale with D). Smaller diameters would have to provide the stiffness through combinations of greater values of L/D and smaller values of D/t to provide greater soil reactions and second moment of area respectively. This suggests that the monopile diameter should be maximised to reduce cost.

Maximising the monopile diameter is further supported in Figure 16 which shows that, in terms of ULS requirements alone, increasing the monopile diameter allows a reduction in L/D; it can be seen that L reduces as D increases. The results thus show that, for the API method, the most cost-efficient monopile will have the largest diameter possible that satisfies the limit state requirements. As the maximum diameter of the monopile is capped by the design space for 10MW at 30m depth, it is expected that even larger diameter monopiles would allow smaller values of L to be used.

The inconsistent shape of the 2D interaction curves (Figure 15) as diameter increases suggests that greater optimisation of monopiles in a wind farm could also be achieved by using the largest diameter possible for the monopile and customising the tower design at every location, so the optimum frequency plane intersects the monopile surface right at the ULS line (line of minimum L/D). In addition, at the ULS line the natural frequency of a wind turbine in the API soil model is relatively invariant with D/t as explained earlier, which would allow the largest value of D/t to be used, thus reducing mass as well as L. However, this is unrealistic as tower designs are currently standardised across wind farms and only monopiles have the flexibility in individual design.

Overall, the results show that the smallest value of L can be achieved by using the largest diameter monopile that satisfies the limit state requirements. The results also show that, while there are FLS and ULS constraints for the API design method in the 10MW, 30m depth scenario, a large limiting factor will be manufacturing capabilities, as larger diameter monopiles would likely allow even smaller values of L.

7.5.2 PISA Results Analysis

Figure 14 shows that the natural frequency of a wind turbine in the PISA soil model is largely independent of L/D above a certain value for each diameter; at constant D/t, natural frequency

	Natural Frequency for $\mathrm{D} = 7.5$m (rad/s)				Proportional Increase for $\mathrm{D} =$10m			
L/D	**6**	**2**	**2**	**6**	**6**	**2**	**2**	**6**
D/t	**60**	**60**	**110**	**110**	**60**	**60**	**110**	**110**
API	1.426	0.6026	0.589	1.179	37.3%	50.7%	52.6%	44.9%
PISA	1.604	1.508	1.273	1.314	35.0%	38.7%	46.4%	44.6%

Table 23: Comparison of wind turbine natural frequency for API and PISA design methods (10MW, 30m Depth)

appears to reach a limit at low values of L/D within the design space. The Figure also suggests that the natural frequency has a negative linear relationship to D/t, which does not appear to change as L/D increases. Increasing the diameter for a monopile using the PISA soil model also resulted in a general increase in natural frequency as expected. Similar to the results obtained for the API method, only requirement 2 of the ULS requirements is failed, which is again dependent on L/D.

The 2D interaction curves (Figure 15) further highlight how the natural frequency of the wind turbine, with respect to L/D, reaches a limit, as the curves become vertical straight lines; i.e. after a certain value of L/D, increasing the length of the monopile into the soil does not increase the stiffness of the structure. The regular spacing of the 2D interaction curves as diameter increases also supports the observation that the relationship between natural frequency and D/t does not change significantly as L/D increases.

The relatively consistent shapes of the 2D interaction curves suggest that there would not be significant motivation to customise the tower design for each location in a wind farm when using the PISA method; changing the intersection of the optimum frequency plane and the monopile surface would only allow larger values of D/t and hence a reduction in mass. Figure 16 shows that the most cost-efficient monopile in the PISA soil model also has the largest possible diameter that satisfies the limit state requirements. However, the 2D interaction curves show that the PISA method appears to be capped by the minimum diameter; the pattern of the interaction curves suggests that a larger design space would allow monopiles of smaller diameter (though larger L/D). Overall, the results for the PISA method show that L can be minimised by using the largest diameter monopile that satisfies the limit state requirements and that the design space is not a major limiting factor for a 10MW wind turbine in 30m depth.

7.5.3 Comparison of API and PISA Results

The most cost-efficient monopile geometries for the two design methods presented in Table 22 show that the PISA method would allow significantly more efficient monopiles to be used; the PISA

method's monopile has an L and mass of just 76.2% and 33.1% of API's respectively.

Table 23 shows the wind turbine natural frequencies for the API and PISA design methods at the extremes of the design space; the differences will arise purely from the different calculations of soil reactions. It can be seen that the API method's calculation of natural frequency is much lower than the PISA method's for the stouter monopiles, supporting the argument that API is overly conservative and inappropriate for smaller aspect ratios; at $D = 7.5$m, $L/D = 2$ and $D/t = 60$, the API method's predicted natural frequency is just 40.0% of the PISA method's, compared to 89.0% at $D = 7.5$m, $L/D = 6$, $D/t = 60$. The greater soil stiffness predicted overall by PISA is expected to arise from the additional soil components it considers in its model (mentioned in Section 3.4).

In terms of how the methods scale with increasing diameter, the proportional increase in natural frequency for the highest values of L/D (Table 23) are relatively similar for the two methods. However, at $L/D = 2$, there is a large variation. Assuming PISA's calculations to be correct, these results show that the API method overestimates the proportional increase in stiffness for stouter monopiles as diameter increases, but that if the soil reaction equations were to be improved, they would scale reasonably similarly to the PISA method for slimmer monopiles.

Comparison of the natural frequency surfaces (Figure 14) further supports concerns of API's applicability to stouter monopiles. As mentioned earlier, D/t does not have much effect on the natural frequency in the API soil model at low values of L/D, whereas the effect of D/t on natural frequency remains relatively constant as L/D is varied for the PISA soil model. At $L/D = 6$, the API method shows a more negative linear relationship between natural frequency and D/t, similar to PISA. This again shows that the API method's calculations at low values of L/D are inaccurate.

Comparing the 2D interaction curves of both methods (Figure 15), at small values of L/D the API interaction curves appear to be similar in shape to the PISA curves but scaled up. The natural frequency predicted by PISA appearing to reach a limit at low values of L/D, with D/t constant, is likely due to the method's significantly greater estimation of soil stiffness, as extending the embedded length of a monopile in relatively stiff soil (under small displacements) would not have much effect on the natural frequency beyond a certain value; only the soil reactions closer to mudline will have a significant effect. As the API method's predicted natural frequency also appears to be reaching a limit at $L/D = 6$, it is believed that if the design space were to be extended, the 2D interaction curves of API would resemble scaled up curves of PISA; if the API monopiles were calculated for $L/D \gg 10$, soil reactions far below mudline would not affect the wind turbine's natural frequency, whereas changes in D/t would.

Both methods are constrained in some way by the ULS and FLS requirements. Considering the largest diameter available to the PISA method, the minimum L/D is predominantly constrained by ULS requirement 2 and D/t is constrained by FLS requirement 3. For API, L/D and D/t are constrained by both requirements 2 and 3, due to the patterns of 2D interaction curves caused by the peak of natural frequency at values of high L/D and low D/t.

Overall, the results also show that PISA can achieve the same wind turbine natural frequency with a monopile of smaller D, t and L, thus supporting the argument that API is more conservative with its soil stiffness calculations. The results also show that maximising the monopile diameter (while still satisfying the limit state requirements) results in more cost-efficient monopiles for both design methods, as both soil reactions and second moment of area scale with D. For the API method, the relationship between natural frequency and D/t is not consistent as L/D varies, and the calculations of natural frequency are much lower than PISA's for low values of L/D, supporting concerns that API is not applicable to stouter monopiles. The implications of these results, besides immediate cost reductions, are that the service life of wind turbines designed using the API method could be significantly increased through better calculation of the natural frequency and hence reduce amplification of cyclic loads.

8. Increasing Water Depth

The design scenario detailed in Section 6 was then adjusted to have different mean water levels to represent offshore sites of greater water depth; four additional scenarios with mean water depths of 35, 40, 45 and 50m were considered. Monopile geometries were selected again, using the API and PISA design methods in a further adjusted PISA project design space, to gain understanding of the potential of each method in future offshore sites.

8.1 Tower Design

The 10MW tower design produced in Section 7 was not changed for the greater depths; instead, the monopile section above mudline in each scenario was extended to provide the same blade clearance and tower clearance above the mean water level. The new tower profiles are shown in Figure 17.

8.2 Results

The CAC was run for $20 \times 20 \times 20$ samples of monopile combinations for each depth scenario and design method; Table 24 shows the most cost-efficient monopile geometries for the API and PISA design methods. Using the data obtained, 2D interaction curves were produced; depths 35m and

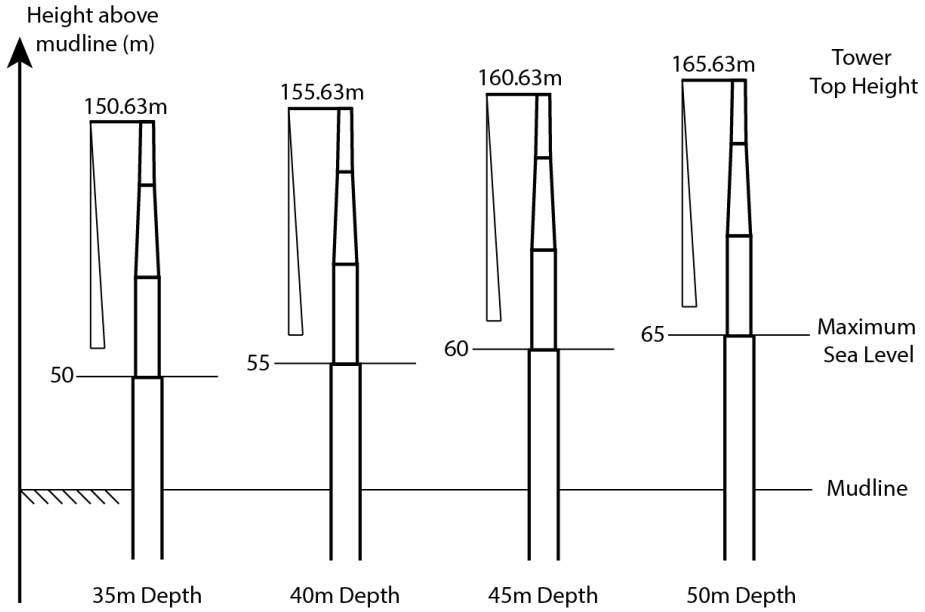

Figure 17: 10MW Tower Profiles for Increasing Depth Scenarios

API						
Depth (m)	D **(m)**	L **(m)**	t **(mm)**	L/D	D/t	**Mass (kg)**
35	10	31.41	149	3.141	67.1	1,122,900
40	10	32.63	160	3.263	62.5	1,267,700
45	10	34.29	157	3.429	63.7	1,307,600
50	10	37.14	157	3.714	63.7	1,416,300
PISA						
Depth (m)	D **(m)**	L **(m)**	t **(mm)**	L/D	D/t	**Mass (kg)**
35	8.11	23.43	82	2.889	98.9	380,620
40	8.50	23.59	93	2.775	91.4	455,140
45	8.81	23.97	98	2.721	89.9	505,020
50	9.10	24.22	98	2.662	92.9	527,270

Table 24: Most cost-efficient 10MW monopile geometries at increasing depths for API (top) and PISA (bottom

50m for the API and PISA methods are shown in Figure 18. The pass/fail records from the CAC showed that, of the two ULS requirements, only requirement 2 (displacement) is failed.

8.3 Analysis

The 2D interaction curves in Figure 18 show that the general patterns of the curves for each method remain the same with increasing depth. However, as depth increases, the interaction curves shift in the L/D - D/t parameter space. This is to be expected as an increase in depth would require an increase of the above-mudline monopile section to achieve the same tower clearance, resulting

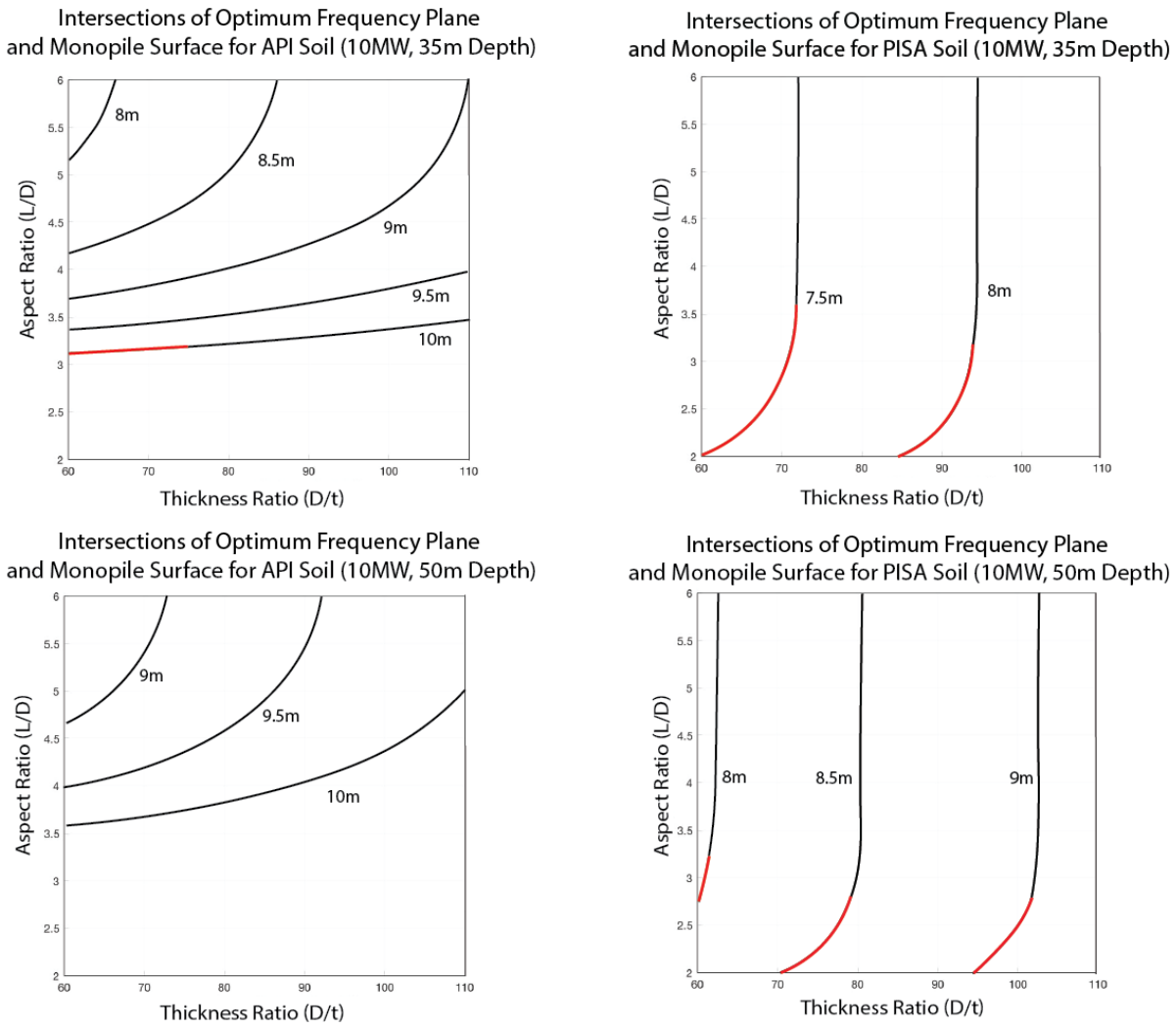

Figure 18: 2D interaction curves for the 10MW wind turbine in 35m (top) and 50m depth (bottom); curves show the intersections of optimum frequency plane and monopile surface for different diameters; black lines show combinations that satisfy all three requirements and red lines show combinations that fail a ULS requirement

in a softening of the structure, and can be visualised as the monopile surfaces shown in Figure 14 moving downwards in the natural frequency axis as depth increases.

8.3.1 API Results Analysis

As depth increases, the softening of the wind turbine appears in the API interaction curves as a shift towards the top-left of the parameter space, as greater foundation stiffness is required to achieve the same optimum natural frequency; at greater depths, the monopile would have to increase in L/D for more soil stiffness, decrease in D/t for a larger second moment of area, or increase in D for a combination of both. The patterns of the 2D interaction curves as depth increases are a result of the varying relationship between natural frequency and D/t as L/D changes, as mentioned in Section

7.5, which changes the interaction curves depending on where the monopile surface intersects the optimum frequency plane.

At 50m depth, only FLS requirement 3 is a constraint and requirement 2 (displacement) is never a limiting factor; extrapolating from the patterns of the previous interaction curves at smaller depths suggest again that more cost-efficient monopiles are possible if larger diameter monopiles are used ($>$10m).

8.3.2 PISA Results Analysis

For PISA, the softening of the structure results in interaction curves that translate horizontally along the D/t axis towards the left with increasing depth, as a result of the roughly negative linear relationship between natural frequency and D/t that does not appear to vary with L/D; this can again be visualised as the monopile surface moving downwards in the frequency axis as depth increases. The curves are generally consistent in shape through different diameters and depths, with the natural frequency again appearing to reach a limit (in the L/D axis) at low values of L/D.

The constraints for the PISA method remains the same as depth increases; the minimum L/D (assuming largest diameter possible) is again constrained predominantly by ULS requirement 2.

8.3.3 Comparison of API and PISA Results

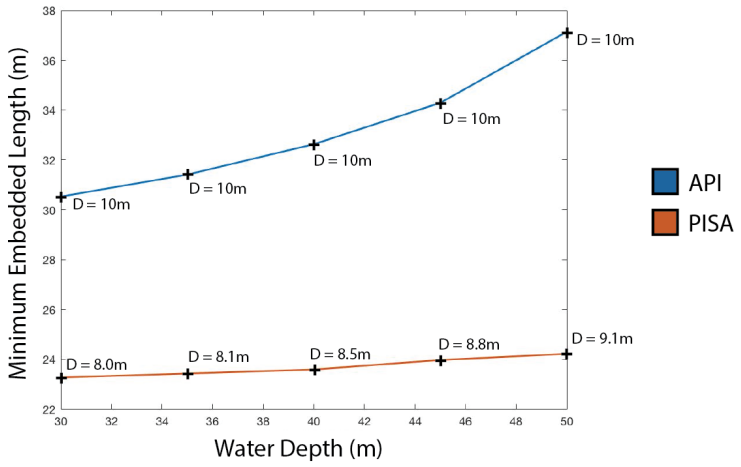

Figure 19: Minimum monopile embedded length L against mean water depth for API (blue) and PISA (red)

The most cost-efficient geometries of both methods presented in Table 24 show that PISA is significantly more economic at increasing depths. At 50m depth, the PISA method monopile has an L and mass of 65% and 37.2% of the API method monopile. It can be seen that the API method monopiles are at the limits of the design space, with $D = 10$ and $D/t \approx 60$, whereas the PISA method

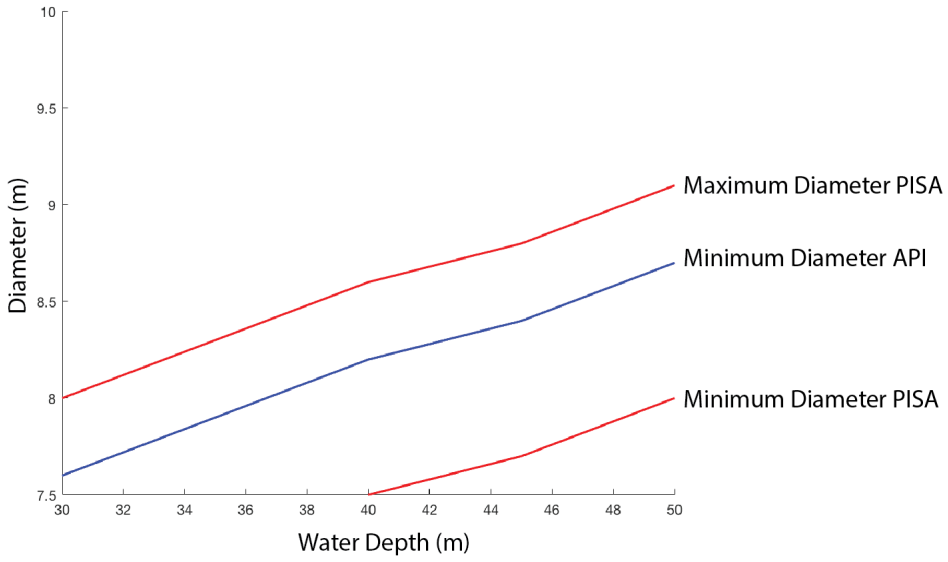

Figure 20: Monopile diameter range against depth for API and PISA methods (10MW)

monopiles are still comfortably within the design space. Figure 19 illustrates further the difference in the two design methods; the gradient of the API curve appears to increase with water depth. As the PISA method monopiles are still well within the design space, the minimum L appears to increase linearly with water depth. The analysis in Section 7.5.3 showed that the API method's natural frequency prediction (and hence stiffness) scaled relatively similarly to the PISA method at high values of L/D but had smaller initial values of stiffness; thus greater increments of monopile parameters would be required to achieve the same stiffness as PISA. It is thus predicted that the API relationship for minimum L against increasing depth in an unrestricted design space would also be linear but of a steeper gradient.

As the API design monopiles in increasing depth require diameters at the end of the design space, it is important to consider that cost-efficiency will not solely depend on L and that reductions in diameter might be more economic, as mentioned in Section 7.1, especially if manufacturing and transportation capabilities do not improve in time. Figure 20 shows the range of diameters monopiles can take as depth increases; the maximum diameter of API method monopiles and some of the data points of the minimum diameter of PISA method monopiles were omitted as they were capped by the design space. While the range of possible API monopile diameters is larger at smaller depths, it is right at the end of the design space. The PISA method's range of possible diameters is smaller due to the FLS constraint described in Section 7.5.3, but it is much closer to diameters of existing monopiles.

Overall, the results show that as depth increases, the API method becomes even less economic compared to PISA, despite scaling relatively similarly at high values of L/D, due to the smaller calcu-

Parameter	12MW	15MW
Rotor Diameter (m)	195.3	218
Tower Top Height from Max Sea Level (m)	126.7	141.61
Rotor and Nacelle Mass (kg)	885,993	1,238,213
Maximum Rotor Speed (rpm)	8.8	7.88
Minimum Rotor Speed (rpm)	5.48	4.89
Optimum Natural Frequency (rad/s)	1.3215	1.1807
Ultimate Load (kN)	3918.8	4898.5

Table 25: 12MW and 15MW Wind Turbine parameters from direct scale up of the 10MW Wind Turbine

lation of soil stiffness. Additionally, the PISA method monopiles are still within current manufacturing capabilities and not at the extremes of the design space like API, making the PISA designs more feasible.

9. Scaling Up

To further develop understanding of the potential of the API and PISA design methods for future wind farms, two theoretical wind turbines rated at 12MW and 15MW were defined for this project so that monopile foundations could be designed and analysed. The new wind turbines were modelled in the design scenarios of varying mean sea level depths detailed in Section 8 (ranging from 30m to 50m) except with updated ultimate loads and FLS requirements for their new power ratings.

9.1 Up Scaling Process

The 12MW and 15MW wind turbines were scaled directly from the 10MW wind turbine designed in Section 7 with the scaling method outlined in the design of the DTU 10MW RWT, described in Section 3.5. Besides updating the key parameters of geometrical dimensions and mass, the new 1P and 3P ranges and ultimate loads had to be recalculated and new tower designs were produced.

9.1.1 Key Parameters

The scaling procedure gives the geometric scaling factors of $\sqrt{12/10}$ and $\sqrt{15/10}$ for the 12MW and 15MW designs respectively; Table 25 shows the key parameters calculated. The rotor diameter, tower top height and tower top weight were obtained through direct scaling from the 10MW design; the tower top height was scaled relative to mean sea level. The rotor speeds were calculated using the assumption of aerodynamic similarity (fixed rotor tip speed) that DTU used when upscaling from the NREL 5MW RWT. Thus, for the maximum and minimum tip speeds of 90.0ms^{-1} and 56.0ms^{-1}, the equivalent rotor speed in rpm, v_r, is calculated from: $v_r = (60v_t)/(D_R\pi)$, where v_t is the tip

speed in ms^{-1} and D_R is the rotor diameter. Finally, the ultimate load on the turbine was calculated assuming that force is proportional to the area swept by the blades; calculation using aero-elastic code was outside the scope of this project. Thus the ultimate force F_u can be obtained from: $F_u = F_{u10MW}(sf)^2$. The values of ultimate load shown in Table 25 include the safety factors of 1.35.

9.1.2 1P and 3P Ranges

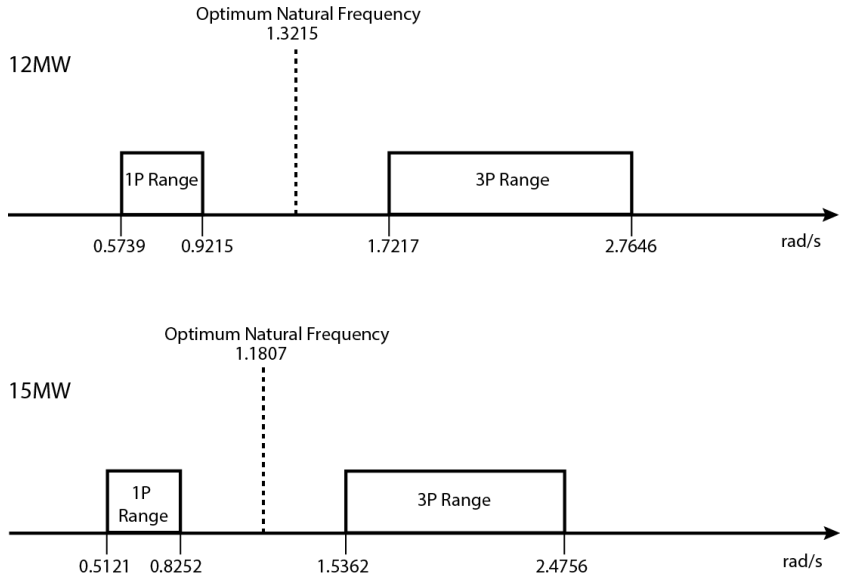

Figure 21: Visualisation of 1P and 3P ranges for 12MW (top) and 15MW (bottom) wind turbines

12MW	**Final Dimensions**		**Dimensions from Direct Scaling**	
Height above Mudline (m)	**D (m)**	**t (mm)**	**D (m)**	**t (mm)**
45	8	88	8.215	87.63
90.25	8	88	8.215	87.36
130.8	6.57	88	6.573	87.63
130.801	6.57	22	6.573	21.91
156.7	6.03	22	6.025	21.91
15MW	**Final Dimensions**		**Dimensions from Direct Scaling**	
Height above Mudline (m)	**D (m)**	**t (mm)**	**D (m)**	**t (mm)**
45	9	98	9.185	97.97
97.36	9	98	9.185	97.97
142.68	7.35	98	7.348	97.97
142.681	7.35	25	7.348	24.49
171.61	6.74	25	6.736	24.49

Table 26: 12MW (top) and 15MW (bottom) tower dimensions at section interfaces

The new rotor speed range required new 1P and 3P ranges to be calculated for the two scaled up wind turbines. Visualisations of the new frequency ranges and optimum natural frequencies are

shown in Figure 21.

9.1.3 Tower Designs

The 12MW and 15MW tower designs were based on the directly up scaled values of the 10MW tower with the following adjustments:

1. Values of diameter and wall thickness were rounded to 3s.f. and 2s.f respectively
2. The diameter of the tower section at the transition to the monopile was reduced relative to its directly scaled geometry in order to increase the available design space, as the monopile diameter cannot be smaller than the tower at the transition piece

The lengths of all tower sections were measured from mean sea level, in order to be consistent with the scaling from DTU's land based tower design. However, the tower starting height was fixed at 45m above mudline - the height of maximum sea level. A yield check was conducted on both tower designs to ensure the ULS was not exceeded. Table 26 shows the final tower dimensions at section interfaces for the two new wind turbines and the orginal directly up scaled values.

12MW Parameter	Range
Diameter D (m)	8-10
Aspect Ratio L/D	2-6
Thickness Ratio D/t	60-110

15MW Parameter	Range
Diameter D (m)	9-10
Aspect Ratio L/D	2-6
Thickness Ratio D/t	60-110

Table 27: Adjusted PISA project design space for 12MW (left) and 15MW (right) wind turbines

API	**12MW**					
Depth (m)	D **(m)**	t **(mm)**	L **(m)**	L/D	D/t	**Mass (kg)**
30	10	167	33.33	3.333	59.9	1,350,622
35	10	141	35.55	3.555	70.9	1,219,516
40	10	167	40.00	4.000	59.9	1,620,909
45	10	153	42.22	4.222	65.4	1,569,675
50	10	153	46.67	4.667	65.4	1,735,119
API	**15MW**					
Depth (m)	D **(m)**	t **(mm)**	L **(m)**	L/D	D/t	**Mass (kg)**
30	10	153	42.22	4.222	65.4	1,569,675
35	10	167	46.67	4.667	59.9	1,891,195
40	10	167	51.11	5.111	59.9	2,071,116
45	10	167	55.56	5.556	59.9	2,251,442
50	-	-	-	-	-	-
PISA	**12MW**					
Depth (m)	D **(m)**	t **(mm)**	L **(m)**	L/D	D/t	**Mass (kg)**
30	8.89	80	24.64	2.772	111.1	428,551
35	9.11	86	25.20	2.766	105.9	482,608
40	9.33	90	25.76	2.761	103.7	528,636
45	9.78	91	26.00	2.658	107.5	565,705
50	10	94	26.50	2.650	106.4	608,931
PISA	**15MW**					
Depth (m)	D **(m)**	t **(mm)**	L **(m)**	L/D	D/t	**Mass (kg)**
30	9.67	93	26.64	2.755	104.0	585,521
35	10	167	26.98	2.698	59.9	1,093,303
40	10	167	27.35	2.735	59.9	1,108,296
45	10	167	28.01	2.801	59.9	1,135,041
50	10	167	29.17	2.917	59.9	1,182,048

Table 28: Most cost-efficient 12MW and 15MW monopile geometries for API (top) and PISA (bottom) methods

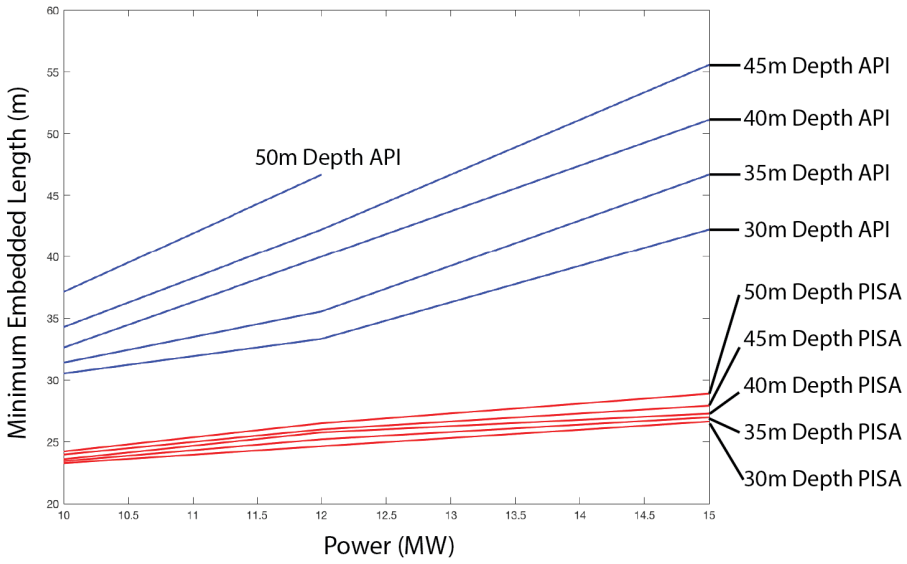

Figure 22: Minimum monopile embedded length against power for varying depth (API and PISA)

9.2 Results

The CAC was used to run 20 $\times$ 20 $\times$ 20 equally spaced samples of monopile geometry combinations within the design spaces for the 12MW and 15MW wind turbines, shown in Table 27; the PISA project design space was again adjusted so the minimum monopile diameter corresponded to the respective tower base diameter. Table 28 shows the most cost-efficient monopile geometries for each wind turbine and depth, obtained from the CAC's results.

To compare cost-efficiency of the design methods, the following Figures were produced: Figure 22

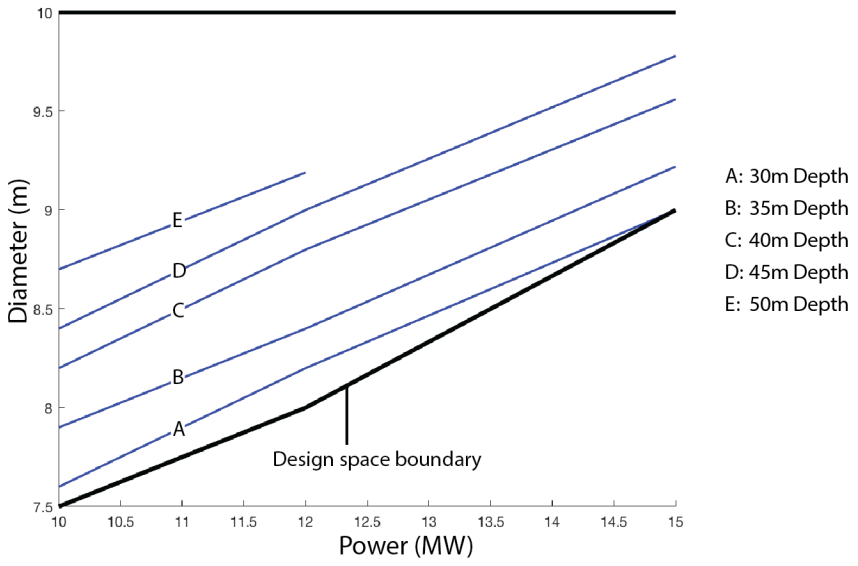

Figure 23: Minimum monopile diameter against power for varying depth (API)

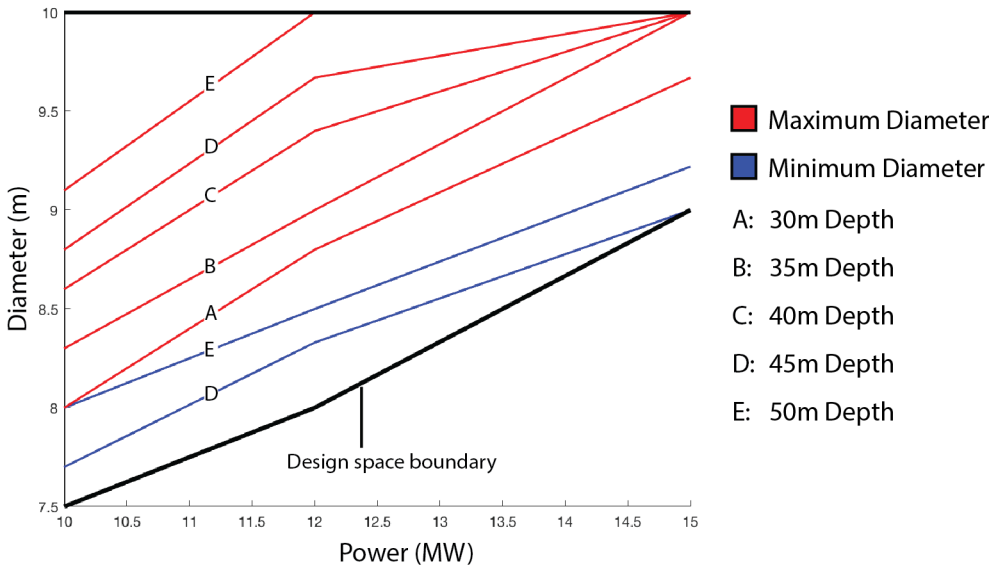

Figure 24: Monopile diameter range against power (PISA)

shows the minimum embedded length against power, plotted for the various depths; Figure 23 shows the minimum API monopile diameter for the different rated wind turbines (the maximum diameters are omitted as they are all capped by the design space); Figure 24 shows the PISA monopile diameter ranges against power plotted for various depth (data points on the design space boundaries were again omitted).

9.3 Analysis

The results show that both design methods are capable of producing monopile designs for the 12MW and 15MW wind turbines at increasing depths, with the exception of API for 15MW at 50m.

9.3.1 API Results Analysis

Table 28 shows that the API design method is again immediately limited by the design space; based on the previous analyses, it is expected that $D > 10$m would allow shorter monopiles that still satisfy the limit state requirements. At 15MW, 45m depth and $D = 10$m, the API method requires a monopile of $L = 115.6$m which is close to the limits of manufacturing capabilities currently being developed; it is thus estimated that 15MW and 45m depth is a rough upper limit for the API method.

9.3.2 PISA Results Analysis

For PISA, the design space becomes a limiting factor for the 12MW wind turbine at 50m depth and the 15MW wind turbine at 35m depth. The effects of this can be seen in Figure 25 which shows the variation of PISA method minimum L with depth for the three wind turbines. The gradient of

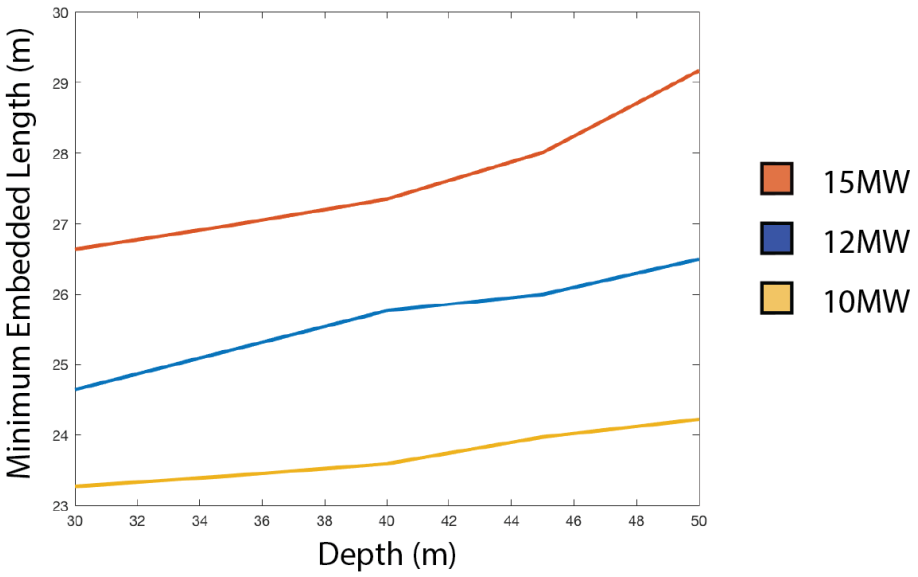

Figure 25: Minimum embedded length against depth (PISA)

the 15MW curve increases slightly, relative to 10MW and 12MW curves, after approximately 35-40m depth when the design space becomes limiting; this would be expected as additional foundation stiffness would be required to compensate for the softening effect of limiting the diameter. In addition, it can be seen that the wall thickness rises significantly at 35m in order for the structure to achieve the same natural frequency with D limited. Extrapolating, it would be expected that, as t and D have reached the maximum values allowed by the design space, the gradient of the L would increase even more greatly with depth.

9.3.3 Comparison of API and PISA Results

Figure 22 shows that the gradient of the L-Power relationship is much greater for API than PISA, thus showing that PISA monopiles are increasingly more cost-efficient at greater depth and scale. Despite the PISA monopile being limited in diameter by the design space at 15MW, its value of L at 45m depth is 50.4% of APIs, which decreases from the value at 12MW, 50m depth, of 56.7%. However, as previously mentioned, this is made possible due to the large increases in wall thickness; at 15MW, 45m depth, PISA's monopile mass is 50.4% of the API's, compared to 37.3% at 30m depth. In terms of versatility, the PISA diameter ranges shown in Figure 24 are comparatively better than the API diameter ranges shown in Figure 23, as they are not as significantly limited by the design space. At 15MW, 45m depth, PISA has a diameter range of 9m to 10m, whereas API's is 9.78m to 10m. Overall, the results show that the PISA method continues to be more cost-efficient than the API method, and more versatile in the range of diameters the PISA monopiles can take. However, the dif-

ference in cost between the two methods begins to reduce at 15MW when the design space becomes limiting as well for the PISA method.

10. Conclusion

The aim of this project is to compare and anlayse the API and PISA monopile design methods, and to explore how the methods and designs evolve with increasing scale and depth. The project aims to determine the cost-efficiency and applicability of the two design methods to future wind turbine designs, as wind energy requires large cost reductions to become economically competitive with traditional sources of energy.

The two design methods, following a limit state design methodology, were used to produce theoretical monopile foundations for three theoretical wind turbines rated at 10, 12 and 15MW, in design scenarios consisting of an offshore clay soil profile with mean water depths of 30, 35, 40, 45 and 50m. New MATLAB code was developed for this project to model the static and dynamic response of a given wind turbine, in order to determine if it satisfies predefined limit state requirements. The 10MW wind turbine is based on the DTU 10MW RWT, from which the 12MW and 15MW models were scaled up using assumptions of geometric and aerodynamic similarity; the three wind turbines exceed the power rating of existing models and hence provide insight into the future potential of the two design methods.

The results show that the API method, compared to the PISA method, significantly underestimates the soil reactions for monopiles of aspect ratios in the range of 2-6, especially at the lower values of aspect ratio. This is expected to be a result of the fewer soil reaction components considered by the API method. The results also suggest that the service life of wind turbines can be improved with the PISA method, as more accurate estimations of natural frequency would reduce interaction with external and operational cyclic loading and hence prevent the accumulation of fatigue damage.

Given current modern manufacturing capabilities being developed, a 15MW wind turbine in 45m depth is an approximate upper limit for the API method. It is expected that PISA method monopiles will satisfy the limit state requirements for even larger wind turbines than those considered, as it is capable of designing monopiles for all the project design scenarios.

It is concluded that the traditional API method significantly underestimates the soil reactions for monopiles of larger diameter and smaller aspect ratio than those used in the formulation of the original *p-y* curves, confirming concerns about its applicability for offshore monopile design. The PISA method can produce monopiles of substantially smaller embedded length, wall thickness and diameter for a given wind turbine, removing a large degree of conservatism from monopile design. As a

result, the API method is considerably less cost-efficient than the newer PISA method, which has the potential to provide economic monopile foundations for offshore wind turbines even larger than those rated at 15MW and to significantly reduce costs in the production of wind energy.

10.1 Further Work

Given more time and resources, several limitations of the project would be addressed to improve the realism and accuracy of the results and conclusions.

For the limit state requirements, the project considered only the yield and mudline deflection for the ULS and the natural frequency of the structure for the FLS. Ideally, additional limit states would be considered, in line with current wind turbine design guidelines, such as buckling of the structure under its self-weight and rotation at mudline. These additional limit state requirements would be incorporated as checks into the developed MATLAB code for the project.

In terms of the scaling up, the realism of the 12MW and 15MW tower designs would be improved by optimising the 12MW and 15MW tower designs using the design process in Section 7. Additionally, as mentioned in Section 3.5, scaling up the ultimate load is also likely an under prediction of the actual ultimate loads; the wind turbine would be analysed using aero-elastic code to determine the ultimate loads more accurately. Finally, a separate tower design optimised for the PISA method would be used in the design of the PISA monopiles to provide a more accurate prediction of the PISA method's capabilities.

References

Bak, C., Zahle, F., Bitsche, R., Kim, T., Yde, A., Henriksen, L. C., Natarajan, A. and Hansen, M. (2013), Description of the DTU 10 MW Reference Wind Turbine, Report, DTU Wind Energy. Report No. I-0092.

Bisoi, S. and Haldar, S. (2014), 'Dynamic analysis of offshore wind turbine in clay considering soil–monopile–tower interaction', *Soil Dynamics and Earthquake Engineering* **63**, 19–35.

Burd, H. (2017), 'Formulation of 1D soil structure interaction models'.

Byrne, B., McAdam, R., Burd, H., Houlsby, G., Martin, C., Zdravković, L., Taborda, D., Potts, D., Jardine, R., Sideri, M. et al. (2015), New design methods for large diameter piles under lateral loading for offshore wind applications, *in* 'Third International Symposium on Frontiers in Offshore Geotechnics', Oslo.

Byrne, B. W., McAdam, R., Burd, H. J., Houlsby, G. T., Martin, C. M., Beuckelaers, W. J. A. P., Zrdavkovic, L., Taborda, D. M. G., Potts, D. M., Jardine, R. J., Ushev, E., Liu, T., Abadias, D., Gavin, K., Igoe, D., Doherty, P., Gretlund, J. S., Andrade, M. P., Wood, A. M., Schroeder, F. C., Turner, S. and Plummer, M. A. L. (2017), New Design Methods for Offshore Wind Turbine Monopiles, *in* 'Eighth International Conference for Offshore Site Investigation and Geotechnics', London.

Davidson, H. L. (1982), Laterally loaded drilled pier research, vol. 1: Design methodology, vol. 2: Research documentation, Report, GAI Consultants Inc.

de Vries, W. E. (2011), UpWind - Final report WP 4.2 - support structure concepts for deep water sites, Report, Delft University of Technology.

DNV-GL (2016), *DNVGL-ST-0126: Support Structures for Wind Turbines*, Det Norske Veritas, Oslo.

Doherty, P. and Gavin, K. (2012), 'Laterally loaded monopile design for offshore wind farms', *Energy* **165**, 7–17.

Germanischer Lloyd (2010), Guideline for the certification of wind turbines, Guideline, Germanischer Lloyd, Hamburg.

Haiderali, A. and Madabhushi, G. (2013), Evaluation of the p-y method in the design of monopiles for offshore wind turbines, *in* 'Offshore Technology Conference', Houston.

Hermans, K. W. and Peeringa, J. M. (2016), Future XL monopile foundation design for a 10MW wind turbine in deep water, Report, ECN Wind Energy. Report No. ECN-E–16-069.

Howatson, A. M., Lund, P. G. and Todd, J. D. (2009), *Engineering Tables and Data*, Department of Engineering Science, University of Oxford, Oxford.

Jonkman, J., Butterfield, S., Musial, W. and Scott, G. (2009), Definition of a 5-MW reference wind turbine for offshore system development, Report, National Renewable Energy Lab.(NREL), United States. Report No. NREL/TP-500-38060.

Junginger, M. and Faaij, A. (2004), 'Cost reduction prospects for the offshore wind energy sector', *Wind Engineering* **28**, 91–118.

Kallehave, D., Byrne, B. W., LeBlanc Thilsted, C. and Mikkelsen, K. K. (2015), 'Optimization of monopiles for offshore wind turbines', *Philosophical Transactions of the Royal Society of London A: Mathematical, Physical and Engineering Sciences* **373**(2035).

Lam, I. P. O. and Martin, G. R. (1986), Seismic design of high-way bridge foundations, Report, US Department of Transportation. Report No. FHWA/RD-86/102.

Matlock, H. (1970), Correlations for design of laterally loaded piles in soft clay, *in* 'The Second Annual Offshore Technology Conference', Houston.

NSC (2015), 'AD 388 Partial factors for material properties for design in the UK'. New Steel Construction. Last accessed: 01/05/2018.
URL: *https://www.steelconstruction.info/images/c/c0/AD-388.pdf*

Pando, M. A., Ealy, C. D., Filz, G. M., Lesko, J. J. and Hoppe, E. J. (2006), A laboratory and field study of composite piles for bridge substructures, Report, Federal Highway Administration, Office of Infrastructure Research and Development. Report No. FHWA-HRT-04-043.

Reese, L. C., Cox, W. R. and Koop, F. D. (1974), Analysis of laterally loaded piles in sand, *in* 'The Sixth Annual Offshore Technology Conference', Houston.

Sieros, G., Chaviaropoulos, P., Srensen, J. D., Bulder, B. H. and Jamieson, P. (2012), 'Upscaling wind turbines: theoretical and practical aspects and their impact on the cost of energy', *Wind Energy* **15**(1), 3–17.

Sif (n.d.), 'Leading european manufacturer of offshore foundations'. Sif Group. Last accessed: 01/05/2018.
URL: *https://sif-group.com/en/about-us/123-leading-european-manufacturer-of-offshore-foundations*

Winkler, E. (1867), *Die lehre von elasticitat und festigkeit*, H. Dominicus, Prague.

Appendix A Risk Assessment

Department of Engineering Science

UNIVERSITY OF OXFORD

Supplementary Questions for 4th Year Project Students

Risk Factor	Answer	Things to Consider	Record details here
Has the checklist covered all the problems that may arise from working with the VDU?	☑ Yes ☐ No		
Are you free from experiencing any fatigue, stress, discomfort or other symptoms which you attribute to working with the VDU or work environment?	☑ Yes ☐ No	Any aches, pains or sensory loss (tingling or pins and needles) in your neck, back shoulders or upper limbs. Do you experience restricted joint movement, impaired finger movements, grip or other disability, temporary or permanently	
Do you take adequate breaks when working at the VDU?	☑ Yes ☐ No	Periods of two minutes looking away from the screen taken every 20 minutes and longer periods every 2 hours Natural breaks for taking a drink and moving around the office answering the phone etc.	
How many hours per day do you spend working with this computer?	☐ 1-2 ☑ 3-4 ☐ 5-7 ☐ 8 or more		
How many days per week do you spend working with this computer?	☐ 1-2 ☑ 3-5 ☐ 6-7		
Please describe your computer usage pattern	Typically 20minute periods followed by breaks for walking around and screen breaks.		